のmRNAや蛋白質の発現レベルが亢進していることが示された[4,16-19]．さらに，ヒト肝細胞癌ではリン酸化を受けた不活性型のYAPが減少していることや，ヒト肝細胞癌，胆管細胞癌，および肝芽腫ではYAPは活性型として，おもに核に存在していることも示された[5,14,17,19,20]．このようにヒト肝癌においてYAPの発現，活性，ならびに核局在の割合が亢進していることが明らかとなってきている．

また，ヒト肝細胞癌の分化度や肝細胞癌患者の血清α-fetoprotein(AFP)値および予後に関する興味深い報告がある．Xuらは，YAP陰性の患者と比較してYAP陽性の肝細胞癌患者は血清AFP値が高いことや癌の分化度が低いことを示した[17]．さらに，YAP陽性の肝細胞癌患者では生存率が有意に低く，5年生存率はYAP陰性の患者は58%であるのに対し，YAP陽性の患者は36%に減少することも報告した．同様にHanらも，YAP陰性の患者と比較して，YAP陽性の肝細胞癌患者では血清AFP値が高いこと，癌の分化度が低いこと，生存率が低いことを示した[21]．以上のように，ヒト肝癌においてもHippo-YAPシグナル経路は肝癌発症の一因を担っていること，YAPは予後マーカーとなることが示唆された．

一方，ヒト胆道の形成とYAPに関する報告もなされている．胆道閉鎖症(BA)は新生児期から乳児期早期に発症する胆汁うっ滞性疾患のひとつであり，胆管の閉塞により重篤な肝障害を引き起こし，早期診断・早期治療が行われなければ死に至る疾患である．2014年にGurdaらはBA以外の原因による胆汁うっ滞性疾患の患児との比較解析によりBAの患児の肝組織では胆管上皮細胞のYAP発現が有意に亢進していることを見出した[22]．これにより，小児の胆汁うっ滞性疾患の鑑別診断を行うにあたりYAPがBAの診断の補助として有用であることが示された．

おわりに

2003年にショウジョウバエにおいて器官サイズを制御するシグナル伝達経路として，Hippo-YAPシグナル経路が同定された．その後10年の間に，マウスを用いた解析によりHippo-YAPシグナル経路の多様な役割が明らかにされてきた．近年ではヒトにおいても，肝癌のみならず卵巣癌や前立腺癌などでHippo-YAPシグナル経路が破綻していることが報告されている[1]．わが国では1981年以降，悪性新生物は死因の第一位であり，その死亡率は増加の一途をたどっている．そのため，今後はHippo-YAPシグナル経路の分子機構の知見を診断や治療に結びつけ，新規癌治療薬開発などが行われていくことが期待される．

謝辞：今回の執筆にあたり多大なご協力をいただいた東京医科歯科大学大学院医歯学総合研究科分子内分泌代謝学分野の小川佳宏先生に深く感謝致します．

文献

1) Harvey, K. F. et al.: *Nat. Rev. Cancer*, **13**: 246-257, 2013.
2) Zhao, B. et al.: *Nat. Cell. Biol.*, **13**: 877-883, 2011.
3) Yimlamai, D. et al.: *Cell*, **157**: 1324-1338, 2014.
4) Dong, J. et al.: *Cell*, **130**: 1120-1133, 2007.
5) Zhou, D. et al.: *Cancer Cell*, **16**: 425-438, 2009.
6) Lu, L. et al.: *Proc. Natl. Acad. Sci. USA*, **107**: 1437-1442, 2010.
7) Song, H. et al.: *Proc. Natl. Acad. Sci. USA*, **107**: 1431-1436, 2010.
8) Lee, K. P. et al.: *Proc. Natl. Acad. Sci. USA*, **107**: 8248-8253, 2010.
9) Nishio, M. et al.: *J. Clin. Invest.*, **112**: 4505-4518, 2012.
10) Benhamouche, S. et al.: *Genes. Dev.*, **24**: 1718-1730, 2010.
11) Zhang, N. et al.: *Dev. Cell*, **19**: 27-38, 2010.
12) Morin-Kensicki, E. M. et al.: *Mol. Cell. Biol.*, **26**: 77-87, 2006.
13) Diego. et al.: *Gastroenterology*, **130**: 1117-1128, 2006.
14) Li, H. et al.: *Liver Int.*, **32**: 38-47, 2012.
15) Zender, L. et al.: *Cell*, **125**: 1253-1267, 2006.
16) Zhang, T. et al.: *Hepatology*, **56**: 2051-2059, 2012.
17) Xu, M. Z. et al.: *Cancer*, **115**: 4576-4585, 2009.
18) Felix, D. et al.: *Gastroenterology*, **144**: 1530-1542, 2013.
19) Zhao, B. et al.: *Genes Dev.*, **21**: 2747-2761, 2007.
20) Tao, J. et al.: *Gastroenterology*, 2014, May 14.(Epub ahead of print)
21) Han, S. X. et al.: *J. Immunol. Res.*, 2014, Apr. 22.(Epub ahead of print)
22) Gurda, G. T. et al.: *Hum. Pathol.*, **45**: 1057-1064, 2014.
23) McClatchey, A. I. et al.: *Genes Dev.*, **12**: 1121-1133, 1998.
24) Avruch, J. et al.: *Br. J. Cancer*, **104**: 24-32, 2011.
25) Camargo, F. D. et al.: *Curr. Biol.*, **17**: 2054-2060, 2007.

J. Biochem. 2014;155(4):235–241 doi:10.1093/jb/mvt114

JB THE JOURNAL OF BIOCHEMISTRY

Overexpression of autotaxin, a lysophosphatidic acid-producing enzyme, enhances cardia bifida induced by hypo-sphingosine-1-phosphate signaling in zebrafish embryo

Received September 30, 2013; accepted December 16, 2013; published online January 21, 2014

Keita Nakanaga[1], Kotaro Hama[1], Kuniyuki Kano[1], Takanao Sato[2], Hiroshi Yukiura[1], Asuka Inoue[1,3], Daisuke Saigusa[4], Hidetoshi Tokuyama[2], Yoshihisa Tomioka[4], Hiroshi Nishina[5], Atsuo Kawahara[6] and Junken Aoki[1,7,*]

[1]Department of Molecular and Cellular Biochemistry, Graduate School of Pharmaceutical Sciences, Tohoku University, 6-3, Aoba, Aramaki, Aoba-ku, Sendai, Miyagi 980-8578, Japan; [2]Laboratory of Medicinal Chemistry, Graduate School of Pharmaceutical Sciences, Tohoku University, 6-3, Aoba, Aramaki, Aoba-ku, Sendai, Miyagi 980-8578, Japan; [3]Presto, JST, 4-1-8 Honcho Kawaguchi, Saitama 332-0012, Japan; [4]Laboratory of Oncology, Pharmacy Practice and Sciences, Graduate School of Pharmaceutical Sciences, Tohoku University, 6-3, Aoba, Aramaki, Aoba-ku, Sendai, Miyagi 980-8578, Japan; [5]Medical Research Institute, Tokyo Medical and Dental University, 1-5-45 Yushima, Bunkyo-ku, Tokyo 113-8510, Japan; [6]Laboratory for Cardiovascular Molecular Dynamics, Riken Quantitative Biology Center, Furuedai 6-2-3, Suita Osaka 565-0874, Japan; and [7]CREST, JST, 4-1-8 Honcho Kawaguchi, Saitama 332-0012, Japan

*Junken Aoki, Department of Molecular and Cellular Biochemistry, Graduate School of Pharmaceutical Sciences, Tohoku University, 6-3, Aoba, Aramaki, Aoba-ku, Sendai, Miyagi 980-8578, Japan. Tel: 81-22-795-6860, Fax: 81-22-795-6859, email: jaoki@m.tohoku.ac.jp

Lysophosphatidic acid (LPA) and sphingosine-1-phosphate (S1P) are second-generation lysophospholipid mediators that exert multiple biological functions through their own cognate receptors. They are both present in the blood stream, activate receptors with similar structures (endothelial differentiation gene receptors), have similar roles in the vasculature and are vasoactive. However, it is unclear whether these lysophospholipid mediators cross-talk downstream of each receptor. Here, we provide *in vivo* evidence that LPA signaling counteracted S1P signaling. When autotaxin (Atx), an LPA-producing enzyme, was overexpressed in zebrafish embryos by injecting *atx* mRNA, the embryos showed cardia bifida, a phenotype induced by down-regulation of S1P signaling. A similar cardiac phenotype was not induced when catalytically inactive Atx was introduced. The cardiac phenotype was synergistically enhanced when antisense morpholino oligonucleotides (MO) against S1P receptor (*s1pr2/mil*) or S1P transporter (*spns2*) was introduced together with *atx* mRNA. The Atx-induced cardia bifida was prominently suppressed when embryos were treated with an *lpar1* receptor antagonist, Ki16425, or with MO against *lpar1*. These results provide the first *in vivo* evidence of cross-talk between LPA and S1P signaling.

Keywords: lysophosphatidic acid/sphingosine-1-phosphate/autotoxin/zebrafish/cardia bifida.

Abbreviations: Atx, autotaxin; *cmlc2*, cardiac myosin light chain 2; Edg, endothelial differentiation gene; hpf, hours post fertilization; LPA, lysophosphatidic acid; LPC, lysophosphatidylcholine; MO, antisense morpholino oligonucleotides; ROCK, Rho kinase; S1P, sphingosine-1-phosphate.

Lysophosphatidic acid (LPA) and sphingosine-1-phosphate (S1P) are lysophospholipid mediators with a number of similar characters. First, the structures of LPA and S1P are quite similar. Second, they are both present in various biological fluids such as plasma, serum and cerebrospinal fluids (*1–4*). Third, they share similar receptors: three LPA receptors (LPA_{1-3}) and all five S1P receptors ($S1P_{1-5}$) belong to the endothelial differentiation gene (Edg) family and share ~35% sequence similarity with each other, although LPA has an additional three receptors belonging to the P2Y family (*5*). Fourth, they have several similar functions that have been demonstrated both *in vivo* and *in vitro*. They both stimulate cell proliferation and motility of various cell types (*6*). They also have critical roles in the vasculature (*7–9*) and are vasoactive (*10*, *11*). Indeed, LPA and S1P regulate blood pressure, both positively and negatively (*12*, *13*). Thus, LPA and S1P appear to share common features and have similar biological roles. However, it is unclear whether there is an interaction between LPA and S1P signaling. Genes involved in LPA and S1P signaling including receptors, producing enzymes, degrading-enzymes and transporters are highly conserved in vertebrates. For example, zebrafish and mammalian autotaxin (Atx) have ~65% amino-acid identity and have similar biochemical and biological roles (*14*). Recent studies of zebrafish and mouse mutants revealed the essential cardiovascular functions of S1P signaling through the S1P transporter *spns2* are conserved from fishes to mammals (*15–19*). These studies have indicated that zebrafish is a useful model organism for elucidating LPA and S1P functions. It may be possible to examine the interaction between LPA signaling and S1P signaling in zebrafish embryos by manipulating the expressions of several genes simultaneously. In this study, we investigated the functional interaction between LPA signaling and S1P signaling by manipulating LPA- and S1P-related genes in zebrafish. Here, we describe the first *in vivo*

evidence showing that LPA signaling affects S1P signaling.

Materials and Methods

Maintenance of zebrafish and drug treatment

Wild-type strain (AB, TU) and transgenic (*cmlc2:mRFP*) were obtained from the Zebrafish International Resource Center (University of Oregon, Eugene, OR) and National BioResource Project, Zebrafish (Riken Brain Research Institute, Wako, Japan). Fish were maintained at 27–28°C under a controlled 13.5-h light/10.5-h dark cycle. Embryos were obtained from natural spawnings and staged according to morphology as described (*20*). Ki16425 was diluted in embryo media supplemented with 1% DMSO and added to zebrafish embryos between 12-h post-fertilization (hpf) and 24 hpf.

mRNA and morpholino injection

The sequences of antisense morpholino oligonucleotides (MO) (Gene Tools, LLC, Corvallis, OR) were designed as previously described (*14*, *16*, *21*). The mRNAs for zebrafish wild-type *atx*, catalytically inactive *atx* (T205A) and mouse wild-type *atx* were synthesized using mMESSAGE MACHINE kit (Ambion, Austin, TX). Morpholinos and synthetic mRNAs were dissolved in water with 0.2% phenol red. Synthetic mRNAs were injected into the blastomere of one cell stage embryos. Morpholinos were injected into the yolk of 1–8 cell stage embryos.

Whole-mount in situ hybridization

An antisense RNA probe labeled with digoxigenin for *cmlc2* was prepared with an RNA labeling kit (Roche Applied Science, Penzberg, Germany). Whole-mount *in situ* hybridization was performed as previously described (*22*).

Evaluation of LPA receptor activation

Activation of LPA receptor was evaluated by a transforming growth factor-α (TGFα) shedding assay as described previously (*23*, *24*). Briefly, each zebrafish LPA receptor gene was introduced into HEK 293T cells together with DNA encoding TGFα fused to alkaline phosphatase. Upon the addition of a ligand for LPA receptors, the TGFα proform expressed on the plasma membrane was cleaved by tumour necrosis factor α converting enzyme (TACE) proteases endogenously expressed in HEK293T cell and thereby released into the culture medium. Then, the activation of LPA receptor was evaluated by measuring the alkaline phosphatase activity in the conditioned medium of the cells.

Measurement of lysophospholipase D activity and Western blotting

Twenty-eight hours after injection, embryos were deyolked as described previously (*14*) and homogenized in lysis buffer [10 mM Tris-HCl (pH 7.4), 10% Triton X-100, 10 μg/ml PMSF, 50 μg/ml Leupeptin, 50 μg/ml Aprotinin] using an ultrasonic homogenizer (Smurt NR-50M; Microtec Nition, Funabashi, Japan). The homogenate was sequentially centrifuged at 21,500 × *g* and the resulting supernatant was collected. Protein concentration was measured with BCA Protein Assay Reagent (Thermo, Waltham, MA) and 5 μg of protein was used for each of lysophospholipase D assay and Western blotting. Lysophospholipase D activity was measured as described previously (*25*). Briefly, the extracts were mixed with 14:0 lysophosphatidylcholine (LPC) (100 mM Tris-HCl, 5 mM $MgCl_2$, 500 mM NaCl, 0.05% Triton X-100, pH 9.0) and incubated for 66 h at 37°C. Liberated choline was quantified using choline oxidase (Wako, Osaka, Japan), peroxidase (TOYOBO, Osaka, Japan) and TOOS reagent (Dojindo, Kumamoto, Japan). The activity was indicated by the generation rate of choline per unit time and protein mass (pmol/μg/h). Western blotting was performed using anti-zebrafish Atx rat polyclonal antibody that was generated as previously described (*14*). Proteins bound to the antibody were visualized with an enhanced chemiluminescence kit (GE Healthcare, Waukesha, WI).

Microscopic analysis and live imaging

Embryos were positioned in 3% methylcellulose (Sigma) on slide glass. Images were captured with a Leica M80 stereomicroscope equipped with Leica DFC425 digital camera (Leica Microsystems, Wetzlar, Germany).

Results

Overexpression of Atx enhances the cardia bifida phenotype in zebrafish embryos

We previously showed that down-regulation of Atx in zebrafish embryos resulted in malformation of the vasculature (*14*). When we tried to rescue the phenotype by injecting mRNA encoding zebrafish *atx* in the embryos, we accidentally found that introduction of *atx* mRNA resulted in an abnormal heart formation (Supplementary movies S1 and S2). Compared with control embryos, blood flow and heart beating were severely impaired at 36 hpf. This phenotype is known as a two-heart or cardia bifida phenotype. In addition, at 54 hpf the tail region of the embryos frequently had blisters (Fig. 1E and F). These are the most characterized phenotypes in previous studies when S1P signal via either S1P receptor (*s1pr2/mil*) or S1P transporter (*spns2*) is attenuated (*15–17*). To examine the cardia bifida phenotype in more detail, we visualized cardiomyocytes by whole-mount *in situ* hybridization using

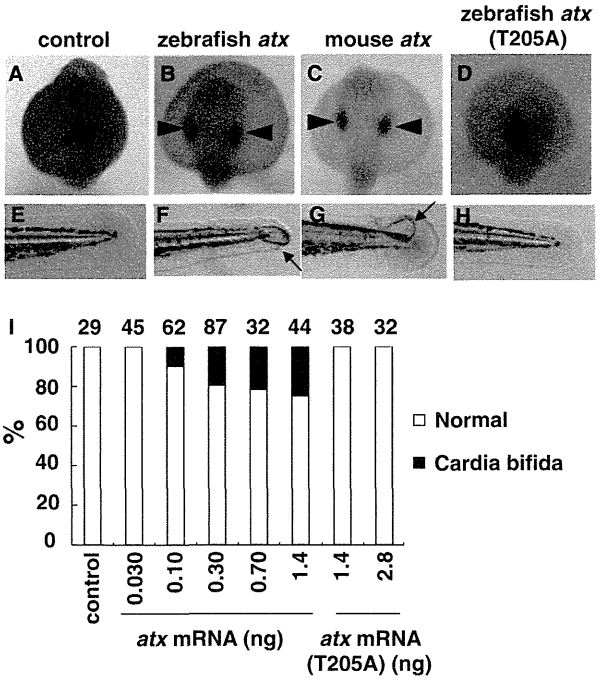

Fig. 1 Overexpression of Atx causes cardia bifida phenotype and tail blisters in zebrafish. Effect of Atx overexpression on the heart formation was examined by whole-mount *in situ* hybridization using *cmlc2* probe (A–D). The phenotypes of cardia bifida (arrowheads) at 24 hpf and tail blister (arrows) at 54 hpf were observed in embryos injected with either wild-type zebrafish *atx* mRNA (B, F) or mouse *atx* mRNA (C, G), which was not observed for catalytically inactive zebrafish *atx* (T205A) mRNA (D, H). (I) Percentage of embryos with cardia bifida phenotype. The number of tested embryos and the amount of mRNA per embryo are listed above and below the graph, respectively. Figures were selected as representative data from three independent experiments.

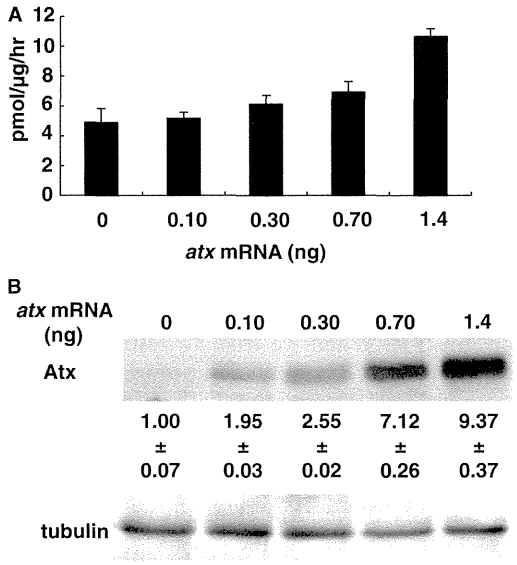

Fig. 2 Expression of Atx in zebrafish embryos injected with *atx* mRNA. Atx enzymatic activity (A) and protein (B) in embryos injected with *atx* mRNA were examined. The enzymatic activity and the protein levels were analyzed by measuring the lysophospholipase D activity in the total lysate of the embryos using LPC as a substrate and Western blot analysis using zebrafish Atx-specific antibody, respectively. The intensity of the bands was determined by densitometrical analysis and the results were shown as the mean ± standard derivation of Atx/tubulin ratios (arbitrary units, $n=3$).

cardiac myosin light chain 2 (*cmlc2*) probe. At 24 hpf, in control embryos, cardiomyocytes were detected in one cluster in the center of the embryos, whereas two clusters of cardiomyocyte were detected in *atx* mRNA-treated embryos (Fig. 1A and B). Similar cardia bifida and tail blister phenotypes were also observed in embryos treated with mouse *atx* mRNA (Fig. 1C and G). Both lysophospholipase D activity and zebrafish Atx protein increased with the dose of injected *atx* mRNA (Fig. 2A and B) and the phenotype was observed when *atx* mRNA higher than 0.03 ng was employed (Fig. 1I). The cardia bifida phenotype required catalytic activity of Atx because either the cardia bifida phenotype or tail blister phenotype was not induced when mRNA for catalytically inactive zebrafish *atx* (T205A) was injected (Fig. 1D, H and I), suggesting that the cardia bifida phenotype was induced via the product of Atx, that is LPA.

Down-regulation of S1P signaling enhances the Atx-induced cardia bifida phenotype

To address the possible link between S1P and LPA signaling, we examined the Atx-induced cardia bifida phenotype when S1P signal was attenuated. We injected *atx* mRNA simultaneously with *mil* or *spns2* MO. First we injected MO for either *mil* or *spns2* and confirmed that significant cardia bifida phenotype was induced at MO concentrations 3.2 ng or more (*mil*), and 5.0 ng or more (*spns2*), but rarely observed at MO concentrations lower than these dosages (Fig. 3A–E and K). Intriguingly, injection of a low dosage of *mil* (1.6 ng) or *spns2* (1.0 ng) MO with *atx* mRNA (0.1 ng) induced an even more severe bifida phenotype (Fig. 3F, G, I, L and M). Indeed, only 7.0% and 3.0% of embryos displayed the cardia bifida phenotype in *mil* and *spns2* MO-treated embryos, respectively, whereas 90% and 60% of embryos displayed the phenotype when *atx* mRNA was co-injected. We observed that the tail blister phenotype was also synergistically induced when *atx* mRNA was co-injected (data not shown). This synergistic effect by *atx* mRNA was catalytically dependent since mRNA for catalytically inactive zebrafish *atx* (T205A) did not show such effect (Fig. 3H, J and N).

LPA_1 mediates Atx-induced cardia bifida

To confirm the involvement of LPA signaling in Atx-induced cardia bifida, we next tried to identify the LPA receptor mediating the Atx-induced cardia bifida. Addition of a LPA_{1-3} antagonist Ki16425 in embryo medium, which also worked on zebrafish Lpar1–3 (*14*), significantly decreased the occurrence frequency of the cardia bifida phenotype induced by injecting *atx* mRNA and *mil* MO in a dose-dependent manner (Fig. 4A). We recently showed that (*R*)-Ki16425 was more potent in antagonizing mammalian LPA_{1-3} than (*S*)-Ki16425 (*26*). We also confirmed that this is also true for zebrafish Lpar1–3 (Fig. 5). Consistent with this, the cardia bifida phenotype was effectively rescued by (*R*)-Ki16425, but not by (*S*)-Ki16425 (Fig. 4B). We further confirmed that the *lpar1* MO partially rescued the cardia bifida phenotype induced by co-injection of *atx* mRNA and *mil* MO (Fig. 4C). The rescue was not observed with *lpar2–6* MO (data not shown). Together, these findings indicate that the cardia bifida phenotype induced by Atx overexpression in zebrafish embryos is mediated by overproduction of LPA and consequent activation of mainly Lpar1. Thus, these results showed that *atx* mRNA treatment affected cardiomyocyte migration that is regulated by S1P signaling in zebrafish embryos at least through Lpar1.

Discussion

In this study, we found that excess LPA signal in zebrafish embryos led to cardia bifida (two heart) phenotype. Because the same phenotype was induced when S1P signaling was down-regulated, we explored the functional interaction between LPA and S1P signaling in the zebrafish heart morphogenesis and found that LPA signaling down-regulated the S1P signaling that led to the cardia bifida phenotype. To our knowledge, this is the first to demonstrate the functional interaction between LPA and S1P signaling.

Among various LPA receptors Lpar1 appeared to be involved in the LPA-induced cardia bifida phenotype. First, the cardia bifida phenotype induced by the co-administration of *atx* mRNA and *mil* MO was almost completely rescued by Ki16425 (Fig. 4A and B), which were found to antagonize all Edg LPA receptors in zebrafish including Lpar1, Lpar2a, Lpar2b and Lpar3 (Fig. 5). Unlike *lpar2a, lpar2b* and *lpar3*, down-regulation of *lpar1* alone rescued the cardia bifida phenotype, showing that Lpar1 is the major LPA receptor involved. Second, we speculate that the functional interaction between LPA and S1P signaling occurs downstream of

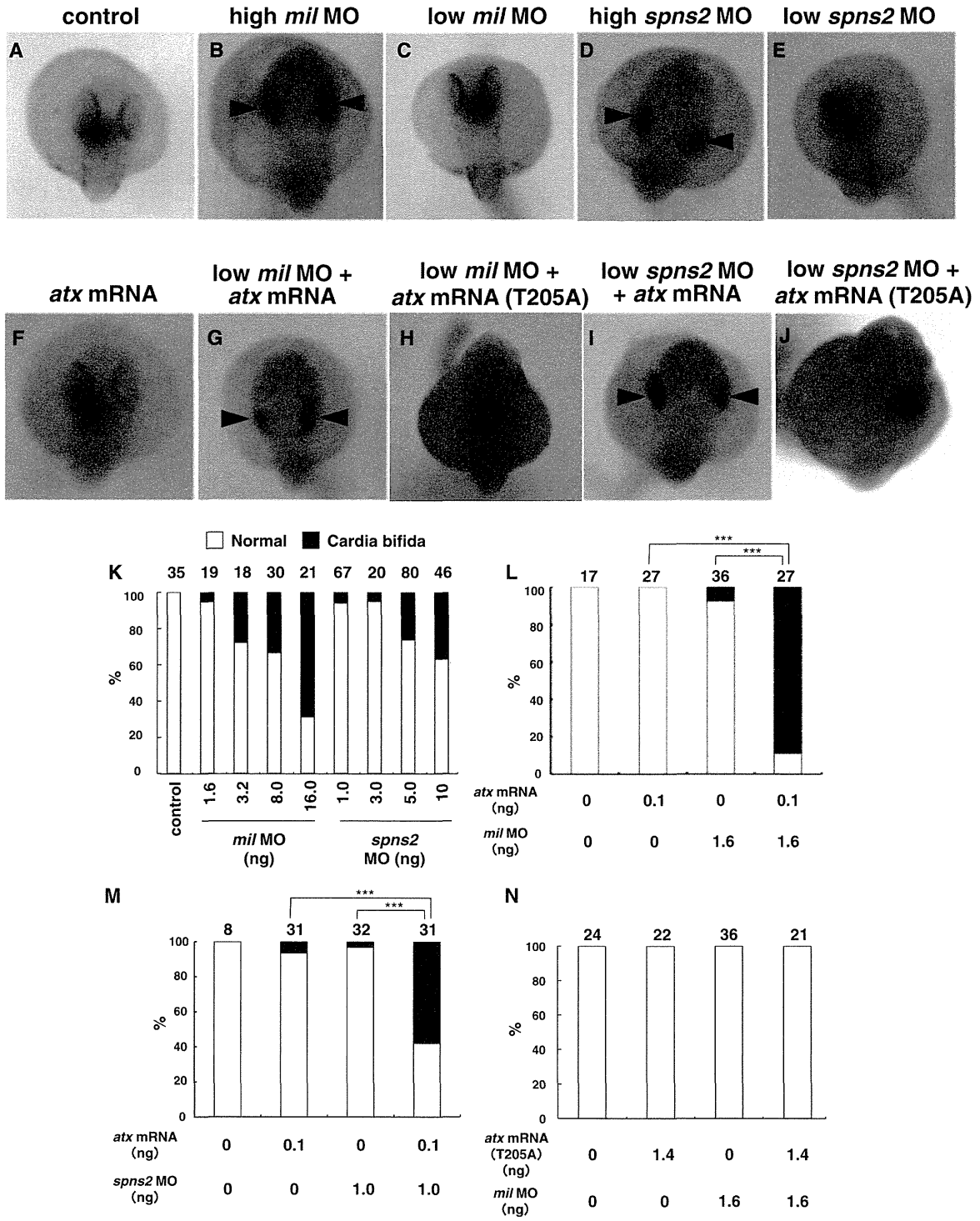

Fig. 3 Cardia bifida phenotype induced by overexpression of Atx was dramatically enhanced when S1P signaling was attenuated. Effect of *mil* and *spns2* down-regulation on cardia bifida phenotype induced by overexpression of Atx was examined. The cardia bifida phenotype was evaluated by whole-mount *in situ* hybridization using *cmlc2* probe at 24 hpf. Cardia bifida phenotype was induced at high concentration of *mil* (8.0 ng) or *spns2* (5.0 ng) MO (B, D). Low *mil* (1.6 ng), low *spns2* (1.0 ng) MO and low *atx* mRNA rarely induced cardia bifida phenotype (C, E, F), whereas co-injection of low *mil* or *spns2* together with *atx* mRNA induced significant cardia bifida phenotype (G, I). These synergistic effects were not observed when catalytically inactive *atx* (T205A) mRNA was co-injected (H, J). (K–N) Percentage of embryos with cardia bifida phenotype was shown. The number of tested embryos, and types of mRNA and MO injected were listed above and below the graph, respectively. K. Dose-dependent increase in the occurrence frequency of the cardia bifida phenotype showing that the phenotype was rarely induced at low dose of MO [1.6 ng (*mil*) and 1.0 ng (*spns2*)]. (L, M) Effect of S1P signal down-regulation on Atx-induced cardia bifida phenotype. Down-regulation of S1P signal was induced either by injecting MO for *mil* (L) or *spns2* (M). Percentage of embryos with cardia bifida phenotype was dramatically increased when *atx* mRNA was injected with MO for *mil* (L) or *spns2* (M) (***$P<0.001$ by χ^2-test). (N) The synergistic effect of *atx* mRNA and S1P-related genes (*mil* and *spns2*) requires catalytic activity of *atx* as catalytically inactive *atx* mRNA did not show the synergistic effect. Figures were selected as representative data from three independent experiments.

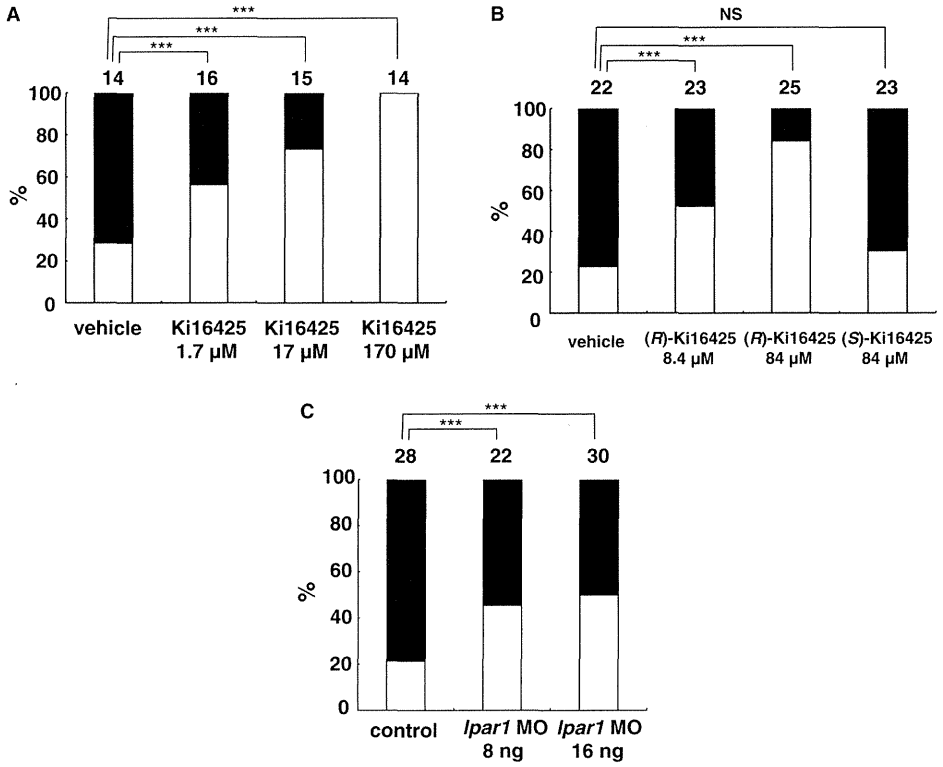

Fig. 4 Cardia bifida phenotype induced by Atx overexpression was mainly mediated by Lpar1. (A, B) Effect of Ki16425 on Atx-induced cardia bifida phenotype in embryos injected with *atx* mRNA (0.1 ng) and *mil* MO (1.6 ng). Ki16425 attenuated cardia bifida phenotype in dose-dependent (A) and enantio-selective (B) manners. (C) Cardia bifida was also recovered by injection of *lpar1* MO (***$P<0.001$ by χ^2-test). NS, not significantly different between the two ($P>0.05$). The number of tested embryos was listed above the graph. Figures were selected as representative data from three independent experiments.

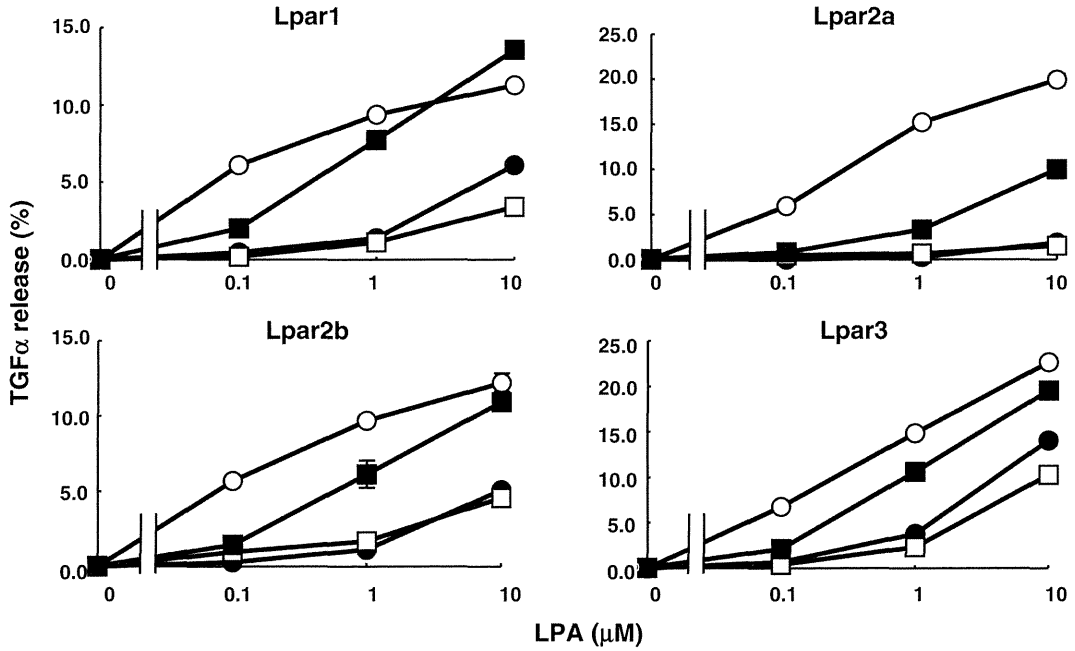

Fig. 5 (*R*)-Ki16425 is potent in antagonizing zebrafish LPA receptors. Activation of the four zebrafish Edg LPA receptors was evaluated by a TGFα shedding assay, in which the activation of each receptor is transduced into TGFα ectodomain shedding. Briefly, HEK293T cells were transfected with cDNAs for each LPA receptor (Lpar1, Lpar2a, Lpar2b and Lpar3), and the amount of alkaline phosphatase (AP)-tagged TGFα released upon LPA stimulation in the presence or absence (open circle) of Ki16425 compounds was determined by measuring AP activity of the culture cell supernatant. (*R*)-Ki16425 (open square) was more potent in antagonizing each LPA receptor than (*S*)-Ki16425 (closed square). The activity of racemic Ki16425 [(*RS*)-Ki16425, closed circle] was also shown. Data represent the means ± standard derivation of triplicate values and are representative of three independent experiments.

each LPA (*lpar1*) and S1P (*mil*) receptor. *Mil* is the zebrafish ortholog of mammalian *s1pr2*. A body of evidence showed that LPA_1 mainly activates $G\alpha_i$-Rac1 signaling whereas $S1P_2$ mainly activates $G\alpha_{12/13}$-RhoA signaling (*5*, *27*). Interestingly, $G\alpha_i$-Tiam1-Rac1 pathway downstream of LPA_1 was shown to inhibit $G\alpha_{12/13}$-mediated RhoA activation in various cell types (*28–30*). Moreover, RhoA and its downstream effector Rho kinase (ROCK) were shown to be essential in cardiac cell migration in both mice and zebrafish (*31*, *32*). Thus, excess Rac1 activation downstream of LPA_1-$G\alpha_i$ signaling might interfere with the RhoA-ROCK activation downstream of *mil*-$G\alpha_{12/13}$ signaling, leading to the cardiac cell migration defect and the two heart phenotype. Third, we speculate that endoderm cells are the cells in which the functional interaction occurs. It was reported that the endoderm cells that are associated with migrating cardiac cells expressed significant amount of *s1pr2*/*mil* mRNA (*15*, *27*). In addition, the endoderm cells are in the vicinity of yolk syncytial layer that expresses *spns2* and thus produces S1P (*16*). *Lpar1* and *s1pr2*/*mil* showed a similar expression pattern in the heart field of developing zebrafish embryos (*21*), supporting the hypothesis.

We also examined if endogenous LPA signaling down-regulates S1P signaling. However, the *mil* or *spns2* MO-induced cardia bifida phenotype was not rescued by *lpar1* MO or Ki16425 (data not shown), suggesting that endogenous LPA_1 signaling does not suppress the S1P signaling in zebrafish cardiac cell migration. Recently, several studies have indicated that excessive Atx-LPA_1 signaling leads to the development of several chronic diseases such as lung fibrosis and arthritis (*33–35*). It is interesting to examine if S1P signaling is suppressed in such diseases and up-regulation of S1P signaling leads to the treatment.

In conclusion, we found two opposite effects of LPA and S1P signaling in zebrafish cardiomyocyte migration. The present results raise the possibility that LPA signaling acts as a modulator of S1P signaling *in vivo*. Further analyses will be necessary to elucidate the precise molecular mechanism of the interaction between LPA and S1P signaling at the cellular level.

Supplementary Data

Supplementary Data are available at *JB* Online.

Funding

This study was supported by Grant in aid for Scientific Research from the Ministry of Education, Culture, Sports, Science, and Technology of Japan (to K.H., A.I. and J.A.), the National Institute of Biomedical Innovation (to J.A.), Japan Science and Technology Agency Precursory Research for Embryonic Science and Technology (PRESTO) (to A.I.), Core Research for Evolutional Science and Technology (CREST) (to J.A.).

Conflict of interest

None declared.

References

1. Tigyi, G. and Miledi, R. (1992) Lysophosphatidates bound to serum albumin activate membrane currents in Xenopus oocytes and neurite retraction in PC12 pheochromocytoma cells. *J. Biol. Chem.* **267**, 21360–21367
2. Sato, K., Malchinkhuu, E., Muraki, T., Ishikawa, K., Hayashi, K., Tosaka, M., Mochiduki, A., Inoue, K., Tomura, H., Mogi, C., Nochi, H., Tamoto, K., and Okajima, F. (2005) Identification of autotaxin as a neurite retraction-inducing factor of PC12 cells in cerebrospinal fluid and its possible sources. *J. Neurochem.* **92**, 904–914
3. Yatomi, Y., Igarashi, Y., Yang, L., Hisano, N., Qi, R., Asazuma, N., Satoh, K., Ozaki, Y., and Kume, S. (1997) Sphingosine 1-phosphate, a bioactive sphingolipid abundantly stored in platelets, is a normal constituent of human plasma and serum. *J. Biochem.* **121**, 969–973
4. Sato, K., Malchinkhuu, E., Horiuchi, Y., Mogi, C., Tomura, H., Tosaka, M., Yoshimoto, Y., Kuwabara, A., and Okajima, F. (2007) HDL-like lipoproteins in cerebrospinal fluid affect neural cell activity through lipoprotein-associated sphingosine 1-phosphate. *Biochem. Biophys. Res. Commun.* **359**, 649–654
5. Chun, J., Hla, T., Lynch, K.R., Spiegel, S., and Moolenaar, W.H. (2010) International Union of Basic and Clinical Pharmacology. LXXVIII. Lysophospholipid receptor nomenclature. *Pharmacol. Rev.* **62**, 579–587
6. Donati, C., Cencetti, F., and Bruni, P. (2013) New insights into the role of sphingosine 1-phosphate and lysophosphatidic acid in the regulation of skeletal muscle cell biology. *Biochim. Biophys. Acta* **1831**, 176–184
7. Tanaka, M., Okudaira, S., Kishi, Y., Ohkawa, R., Iseki, S., Ota, M., Noji, S., Yatomi, Y., Aoki, J., and Arai, H. (2006) Autotaxin stabilizes blood vessels and is required for embryonic vasculature by producing lysophosphatidic acid. *J. Biol. Chem.* **281**, 25822–25830
8. Liu, Y., Wada, R., Yamashita, T., Mi, Y., Deng, C.X., Hobson, J.P., Rosenfeldt, H.M., Nava, V.E., Chae, S.S., Lee, M.J., Liu, C.H., Hla, T., Spiegel, S., and Proia, R.L. (2000) Edg-1, the G protein-coupled receptor for sphingosine-1-phosphate, is essential for vascular maturation. *J. Clin. Invest.* **106**, 951–961
9. Sumida, H., Noguchi, K., Kihara, Y., Abe, M., Yanagida, K., Hamano, F., Sato, S., Tamaki, K., Morishita, Y., Kano, M.R., Iwata, C., Miyazono, K., Sakimura, K., Shimizu, T., and Ishii, S. (2010) LPA4 regulates blood and lymphatic vessel formation during mouse embryogenesis. *Blood* **116**, 5060–5070
10. Tokumura, A., Fukuzawa, K., and Tsukatani, H. (1978) Effects of synthetic and natural lysophosphatidic acids on the arterial blood pressure of different animal species. *Lipids* **13**, 572–574
11. Sugiyama, A., Yatomi, Y., Ozaki, Y., and Hashimoto, K. (2000) Sphingosine 1-phosphate induces sinus tachycardia and coronary vasoconstriction in the canine heart. *Cardiovasc. Res.* **46**, 119–125
12. Tokumura, A., Yotsumoto, T., Masuda, Y., and Tanaka, S. (1995) Vasopressor effect of lysophosphatidic acid on spontaneously hypertensive rats and Wistar Kyoto rats. *Res. Commun. Mol. Pathol. Pharmacol.* **90**, 96–102
13. Sanna, M.G., Liao, J., Jo, E., Alfonso, C., Ahn, M.Y., Peterson, M.S., Webb, B., Lefebvre, S., Chun, J., Gray, N., and Rosen, H. (2004) Sphingosine 1-phosphate (S1P) receptor subtypes S1P1 and S1P3, respectively, regulate lymphocyte recirculation and heart rate. *J. Biol. Chem.* **279**, 13839–13848
14. Yukiura, H., Hama, K., Nakanaga, K., Tanaka, M., Asaoka, Y., Okudaira, S., Arima, N., Inoue, A.,

Hashimoto, T., Arai, H., Kawahara, A., Nishina, H., and Aoki, J. (2011) Autotaxin regulates vascular development via multiple lysophosphatidic acid (LPA) receptors in zebrafish. *J. Biol. Chem.* **286**, 43972–43983

15. Kupperman, E., An, S., Osborne, N., Waldron, S., and Stainier, D.Y. (2000) A sphingosine-1-phosphate receptor regulates cell migration during vertebrate heart development. *Nature* **406**, 192–195
16. Kawahara, A., Nishi, T., Hisano, Y., Fukui, H., Yamaguchi, A., and Mochizuki, N. (2009) The sphingolipid transporter spns2 functions in migration of zebrafish myocardial precursors. *Science* **323**, 524–527
17. Osborne, N., Brand-Arzamendi, K., Ober, E.A., Jin, S.W., Verkade, H., Holtzman, N.G., Yelon, D., and Stainier, D.Y. (2008) The spinster homolog, two of hearts, is required for sphingosine 1-phosphate signaling in zebrafish. *Curr. Biol.* **18**, 1882–1888
18. Fukuhara, S., Simmons, S., Kawamura, S., Inoue, A., Orba, Y., Tokudome, T., Sunden, Y., Arai, Y., Moriwaki, K., Ishida, J., Uemura, A., Kiyonari, H., Abe, T., Fukamizu, A., Hirashima, M., Sawa, H., Aoki, J., Ishii, M., and Mochizuki, N. (2012) The sphingosine-1-phosphate transporter Spns2 expressed on endothelial cells regulates lymphocyte trafficking in mice. *J. Clin. Invest.* **122**, 1416–1426
19. Hisano, Y., Kobayashi, N., Yamaguchi, A., and Nishi, T. (2012) Mouse SPNS2 functions as a sphingosine-1-phosphate transporter in vascular endothelial cells. *PLoS One* **7**, e38941
20. Kimmel, C.B., Ballard, W.W., Kimmel, S.R., Ullmann, B., and Schilling, T.F. (1995) Stages of embryonic development of the zebrafish. *Dev. Dyn.* **203**, 253–310
21. Lee, S.J., Chan, T.H., Chen, T.C., Liao, B.K., Hwang, P.P., and Lee, H. (2008) LPA1 is essential for lymphatic vessel development in zebrafish. *FASEB J.* **22**, 3706–3715
22. Thisse, C. and Thisse, B. (2008) High-resolution in situ hybridization to whole-mount zebrafish embryos. *Nat. Protoc.* **3**, 59–69
23. Inoue, A., Arima, N., Ishiguro, J., Prestwich, G.D., Arai, H., and Aoki, J. (2011) LPA-producing enzyme PA-PLA$_1\alpha$ regulates hair follicle development by modulating EGFR signalling. *EMBO J.* **30**, 4248–4260
24. Inoue, A., Ishiguro, J., Kitamura, H., Arima, N., Okutani, M., Shuto, A., Higashiyama, S., Ohwada, T., Arai, H., Makide, K., and Aoki, J. (2012) TGFα shedding assay: an accurate and versatile method for detecting GPCR activation. *Nat. Methods* **9**, 1021–1029
25. Umezu-Goto, M., Kishi, Y., Taira, A., Hama, K., Dohmae, N., Takio, K., Yamori, T., Mills, G.B., Inoue, K., Aoki, J., and Arai, H. (2002) Autotaxin has lysophospholipase D activity leading to tumor cell growth and motility by lysophosphatidic acid production. *J. Cell Biol* **158**, 227–233
26. Sato, T., Sugimoto, K., Inoue, A., Okudaira, S., Aoki, J., and Tokuyama, H. (2012) Synthesis and biological evaluation of optically active Ki16425. *Bioorg. Med. Chem. Lett.* **22**, 4323–4326
27. Ye, D. and Lin, F. (2013) S1pr2/Gα13 signaling controls myocardial migration by regulating endoderm convergence. *Development* **140**, 789–799
28. Van Leeuwen, F.N., Olivo, C., Grivell, S., Giepmans, B.N., Collard, J.G., and Moolenaar, W.H. (2003) Rac activation by lysophosphatidic acid LPA1 receptors through the guanine nucleotide exchange factor Tiam1. *J. Biol. Chem.* **278**, 400–406
29. Leeuwen, F.N., Kain, H.E., Kammen, R.A., Michiels, F., Kranenburg, O.W., and Collard, J.G. (1997) The guanine nucleotide exchange factor Tiam1 affects neuronal morphology; opposing roles for the small GTPases Rac and Rho. *J. Cell Biol* **139**, 797–807
30. Sander, E.E., ten Klooster, J.P., van Delft, S., van der Kammen, R.A., and Collard, J.G. (1999) Rac downregulates Rho activity: reciprocal balance between both GTPases determines cellular morphology and migratory behavior. *J. Cell Biol* **147**, 1009–1022
31. Wei, L., Roberts, W., Wang, L., Yamada, M., Zhang, S., Zhao, Z., Rivkees, S.A., Schwartz, R.J., and Imanaka-Yoshida, K. (2001) Rho kinases play an obligatory role in vertebrate embryonic organogenesis. *Development* **128**, 2953–2962
32. Matsui, T., Raya, A., Kawakami, Y., Callol-Massot, C., Capdevila, J., Rodríguez-Esteban, C., and Izpisúa Belmonte, J.C. (2005) Noncanonical Wnt signaling regulates midline convergence of organ primordia during zebrafish development. *Genes Dev.* **19**, 164–175
33. Tager, A.M., LaCamera, P., Shea, B.S., Campanella, G.S., Selman, M., Zhao, Z., Polosukhin, V., Wain, J., Karimi-Shah, B.A., Kim, N.D., Hart, W.K., Pardo, A., Blackwell, T.S., Xu, Y., Chun, J., and Luster, A.D. (2008) The lysophosphatidic acid receptor LPA1 links pulmonary fibrosis to lung injury by mediating fibroblast recruitment and vascular leak. *Nat. Med.* **14**, 45–54
34. Oikonomou, N., Mouratis, M.A., Tzouvelekis, A., Kaffe, E., Valavanis, C., Vilaras, G., Karameris, A., Prestwich, G.D., Bouros, D., and Aidinis, V. (2012) Pulmonary autotaxin expression contributes to the pathogenesis of pulmonary fibrosis. *Am. J. Respir. Cell Mol. Biol.* **47**, 566–574
35. Nikitopoulou, I., Oikonomou, N., Karouzakis, E., Sevastou, I., Nikolaidou-Katsaridou, N., Zhao, Z., Mersinias, V., Armaka, M., Xu, Y., Masu, M., Mills, G.B., Gay, S., Kollias, G., and Aidinis, V. (2012) Autotaxin expression from synovial fibroblasts is essential for the pathogenesis of modeled arthritis. *J. Exp. Med.* **209**, 925–933

MCB
Journals.ASM.org

Screening with a Novel Cell-Based Assay for TAZ Activators Identifies a Compound That Enhances Myogenesis in C2C12 Cells and Facilitates Muscle Repair in a Muscle Injury Model

Zeyu Yang,[a,b] Kentaro Nakagawa,[a] Aradhan Sarkar,[a] Junichi Maruyama,[a] Hiroaki Iwasa,[a] Yijun Bao,[a,c] Mari Ishigami-Yuasa,[d] Shigeru Ito,[e] Hiroyuki Kagechika,[d,e] Shoji Hata,[f] Hiroshi Nishina,[f] Shinya Abe,[g] Masanobu Kitagawa,[g] Yutaka Hata[a,h]

Department of Medical Biochemistry, Graduate School of Medical and Dental Sciences, Tokyo Medical and Dental University, Tokyo, Japan[a]; Department of Ultrasound, Shengjing Hospital of China Medical University, Shenyang, China[b]; Department of Neurosurgery, First Hospital of China Medical University, Shenyang, China[c]; Chemical Biology Screening Center[d] and Institute of Biomaterials and Bioengineering,[e] Tokyo Medical and Dental University, Tokyo, Japan; Department of Developmental and Regenerative Biology, Medical Research Institute, Tokyo Medical and Dental University, Tokyo, Japan[f]; Department of Comprehensive Pathology, Graduate School of Medical and Dental Sciences, Tokyo Medical and Dental University, Tokyo, Japan[g]; Center for Brain Integration Research, Tokyo Medical and Dental University, Tokyo, Japan[h]

The transcriptional coactivator with a PDZ-binding motif (TAZ) cooperates with various transcriptional factors and plays various roles. Immortalized human mammalian epithelial MCF10A cells form spheres when TAZ is overexpressed and activated. We developed a cell-based assay using sphere formation by TAZ-expressing MCF10A cells as a readout to screen 18,458 chemical compounds for TAZ activators. Fifty compounds were obtained, and 47 were confirmed to activate the TAZ-dependent TEAD-responsive reporter activity in HEK293 cells. We used the derived subset of compounds as a TAZ activator candidate minilibrary and searched for compounds that promote myogenesis in mouse C2C12 myoblast cells. In this study, we focused on one compound, IBS008738. IBS008738 stabilizes TAZ, increases the unphosphorylated TAZ level, enhances the association of MyoD with the myogenin promoter, upregulates MyoD-dependent gene transcription, and competes with myostatin in C2C12 cells. TAZ knockdown verifies that the effect of IBS008738 depends on endogenous TAZ in C2C12 cells. IBS008738 facilitates muscle repair in cardiotoxin-induced muscle injury and prevents dexamethasone-induced muscle atrophy. Thus, this cell-based assay is useful to identify TAZ activators with a variety of cellular outputs. Our findings also support the idea that TAZ is a potential therapeutic target for muscle atrophy.

The transcriptional coactivator with a PDZ-binding motif (TAZ, also called WWTR1) was identified as a 14-3-3-binding protein (1–3). It is similar to Yes-associated protein 1 (YAP1) in its molecular structure, which consists of an N-terminal TEAD-binding domain, one or two WW domains, and a transcriptional activation domain (4). The Hippo pathway is a tumor suppressor signaling pathway that was initially identified in *Drosophila* (2, 5, 6). TAZ is phosphorylated at four sites by large tumor suppressor kinase 1 (LATS1) and LATS2, which are core kinases of the Hippo pathway (1–3). Phosphorylated TAZ is trapped by 14-3-3, is recruited from the nucleus to the cytoplasm, and undergoes protein degradation (1–3). In this way, the Hippo pathway negatively regulates TAZ. In addition to the Hippo pathway, TAZ is regulated by cell junction proteins such as ZO-1, ZO-2, and angiomotin (7–10). Recent studies have revealed that TAZ is under the control of the actin cytoskeleton and the mechanical stretch (11–13). Moreover, Wnt signaling stabilizes TAZ (14–16). Conversely, cytoplasmic TAZ binds β-catenin and Dishevelled (DVL) and inhibits β-catenin nuclear localization and DVL phosphorylation to negatively regulate the Wnt pathway. This shows that TAZ plays a pivotal role in the cross talk between the Hippo pathway and the Wnt pathway.

In human cancers, the Hippo pathway is frequently compromised, resulting in TAZ hyperactivity (6). TAZ gene amplification is also detected in cancers (17–21). TAZ hyperactivity causes epithelial-mesenchymal transitions (EMT) and provides cancer cells with stemness (22–26). Hence, TAZ is considered a potential cancer therapeutic target. The transforming ability of TAZ is attributed mostly to the interaction with TEAD and Wbp2 (22, 27–29). Besides TEAD and Wbp2, TAZ interacts with numerous transcriptional factors. TAZ interacts with thyroid transcription factor 1, Pax8, and T-box transcription factor 5 and is important for lung, thyroid, heart, and limb development (30, 31). It also interacts with p300 (31). In human embryonic stem cells, TAZ interacts with SMAD2, -3, and -4 and is essential for the maintenance of self-renewal (16, 32, 33). In mesenchymal stem cells, TAZ interacts with peroxisome proliferator-activated receptor γ and Runx2 to suppress adipogenesis and promote osteogenesis (34, 35). In skeletal muscles, TAZ interacts with transcriptional factors that are implicated in myogenesis. It binds the key myogenic regulators Pax3 and MyoD (36, 37). TEAD binds to the so-called MCAT elements (muscle C, A, and T; 5′-CATTCC-3′) in muscle-specific genes such as that for myogenin (38). Although SMAD2 and -3, which are TAZ interactors, mediate the inhibitory signal of myostatin in muscle cells (39), TAZ is overall regarded as a myogenesis-promoting factor. This makes a sharp contrast with YAP1, whose activation induces muscle atrophy (40, 41).

Received 8 October 2013 **Returned for modification** 31 October 2013
Accepted 11 February 2014
Published ahead of print 18 February 2014
Address correspondence to Yutaka Hata, yuhammch@tmd.ac.jp.
Supplemental material for this article may be found at http://dx.doi.org/10.1128/MCB.01346-13.

doi:10.1128/MCB.01346-13

Sarcopenia is a skeletal muscle atrophy associated with ageing (42). Sarcopenia deprives elderly populations of the ability to live independently and will be a major health concern in industrialized countries. Appropriate exercise and nutrition are key factors in the prevention and treatment of sarcopenia. However, the development of drugs to increase skeletal muscles is also required. Satellite cells are considered skeletal muscle progenitor cells and a major source to regenerate muscle tissue in adults. Although the role of TAZ in the maintenance of muscle satellite cells remains to be clarified, considering the potential role of TAZ in myogenesis, we expected that TAZ activators are beneficial for the therapy of sarcopenia. We established a cell-based assay for TAZ activators, screened 18,458 chemical compounds, and obtained 50 TAZ activator candidates. We subsequently selected compounds that promote myogenesis in mouse C2C12 myoblast cells and finally focused on one compound that facilitates muscle repair in an injury model and prevents dexamethasone-induced muscle atrophy.

MATERIALS AND METHODS

DNA constructs and virus production. The pLenti-EF-ires-blast, pClneoFH, and pClneoHA vectors were described previously (43–45). A TAZ SA mutant, in which serine 89 is mutated to alanine, was prepared by the PCR method. pLenti-EF-FH-TAZ and TAZ SA-ires-blast were prepared by subcloning NheI/SalI fragments from pClneoFH-TAZ and pClneoFH-TAZ S89A into the pLenti-EF-ires-blast vector. The BLOCK-iT Pol II miR RNA interference (RNAi) expression vector kit (Invitrogen) was used to generate pcDNA knockdown constructs for human LATS1 and LATS2. The target sequences were a 1,074-bp site of LATS1 (AF104413.1) and a 1,598-bp site of LATS2 (AF207547.1). The annealing oligonucleotides were ligated into the pcDNA 6.2-GW/miR vector according to the manufacturer's protocol to generate pcDNA 6.2 LATS1 KD and pcDNA 6.2 LATS2 KD. A BamHI/XhoI fragment was isolated from pcDNA 6.2 LATS2 KD and ligated into the BglII/XhoI sites of pcDNA 6.2 LATS1 KD to generate pcDNA 6.2 LATS1/2 KD. PCR was performed on pBudCE with primers H1674 (5′-ATCGATGTCGAGCTAGCTTCGTGAG-3′) and H1675 (5′-ACTAGTCTCGAGACCACGTGTTCACGACACC-3′) to amplify the elongation factor (EF) promoter. The PCR product was digested with ClaI and SpeI and ligated into the same sites of pLenti4/TO/V5-DEST to replace the pCMV/VO promoter with the EF promoter and to generate pLenti4-EF/V5-DEST. The pLenti-EmGFP LATS1/2 KD vector was generated by using the ViraPower T-REx lentiviral expression system from pcDNA 6.2 LATS1/2 KD and pLenti4-EF/V5-DEST. The NheI/NotI fragment from pBudCE4.1 was ligated into the XbaI/NotI sites of pQCXIP (Clontech) to generate pQCXIP EF. The linker (H3142 [5′-GGCCGCTCGAGTTTAAACAATTGGATCC-3′] and H-3143 [5′-AATTGGATCCAATTGTTTAAACTCGAGC-3′]) was subcloned into the NotI/EcoRI sites to generate pQCXIP EF H3142/H3143. The BglII/NotI fragment from pClneo mCherry was ligated into the BglII/NotI sites of pQCXIP EF H3142/H3143 to generate pQCXIP mCherry, which was digested with BamHI/EcoRV, filled in, and religated to remove the internal ribosome entry sites and the puromycin resistance gene. The resulting vector was named pQCXI mCherry. pLenti-siRNA-GFP (Applied Biological Materials Inc.) was digested with SpeI/MluI. The isolated green fluorescent protein (GFP)-2A-puro fragment was subcloned into NheI/MluI sites of pClneo to generate pClneo GFP-2A-puro, which was subsequently digested with BglII/MluI. The isolated fragment was ligated into the BglII/MluI sites of pQCXI mCherry to generate pQCXI GFP2A-puromycin. WWTR1 mouse pRFP-RS short hairpin RNA (shRNA) (TF505533, 561750; OriGene) was purchased, and PCR was performed with primers H3163 (5′-CAATTGAATTCCCCAGTGGAAAGACGCGCA-3′) and H3164 (5′-ACGCGTCTCGAGCCTGGGGACTTTCACAC-3′) to amplify the U6 promoter and the target sequence. The PCR product was subcloned into the TAKN2 vector (BioDynamics Laboratory Inc.) and digested with MluI/NotI. The isolated fragment was ligated into the MluI/NotI sites of pQCXI GFP2A-puromycin. The vector was cotransfected with the pCL10A-1 retrovirus packaging vector into HEK293 cells to generate retrovirus for mouse TAZ knockdown. Lentivirus was generated as described previously (46).

Antibodies and reagents. The rat anti-YAP monoclonal antibody used was described previously (43). The following antibodies and reagents were obtained from commercial sources. The mouse anti-TAZ (560235), mouse anti-MyoD (554130), mouse anti-poly(ADP-ribose) polymerase (anti-PARP) (51-6639GR), mouse antifibronectin (610077), mouse anti-E-cadherin (610181), and mouse anti-N-cadherin (610921) antibodies and Matrigel were from BD Pharmingen. The rabbit antimyogenin (sc-576), rabbit anti-MyoD (sc-760), and mouse antivimentin (sc-6260) antibodies were from Santa Cruz. The mouse anti-myosin heavy chain (anti-MHC) (MF20), mouse anti-Pax7, and mouse anti-Pax3 antibodies were from the Developmental Studies Hybridoma Bank, University of Iowa. The rabbit antilaminin (L9293), mouse anti-α-tubulin (T9026), and mouse anti-FLAG M2 (F3165) antibodies; Hoechst 33342; *Naja mossambica* cardiotoxin; dexamethasone (C9759); epidermal growth factor (E9644); insulin (I5500), and 3-(4,5-dimethylthiazol-2-yl)-2,5-diphenyltetrazolium bromide (MTT) were from Sigma-Aldrich. Basic fibroblast growth factor (064-04541) and Phos-tag acrylamide were from Wako Chemicals. The mouse antimyogenin antibody (ab1835) was from Abcam. The mouse antihemagglutinin (anti-HA) antibody was from Roche. The mouse antiactin (clone 4) and mouse antipuromycin (clone 12D10) antibodies were from Millipore. The rabbit anti-TEAD4 antibody (APR38726_P050) was from Aviva. The goat anti-Pax3 antibody (GWB-3AE0a5) was from Genway Biotech Inc. The recombinant myostatin (788-G8-010) was from R&D Systems.

Cell culture and transfection. HEK293, A431, and HCT116 cells were cultured in Dulbecco's modified Eagle medium (DMEM) containing 10% fetal bovine serum (FBS) and 10 mM HEPES-NaOH at pH 7.4 under 5% CO_2 at 37°C. MCF10A cells were cultured in DMEM–F-12 supplemented with 5% horse serum (Invitrogen), 20 ng/ml epidermal growth factor, 0.5 μg/ml hydrocortisone, and 10 μg/ml insulin. DNA transfection was performed with Lipofectamine 2000 (Invitrogen). MCF10A-TAZ and MCF10A-TAZ SA cells were prepared with pLenti-EF-FH-TAZ-ires-blast and pLenti-EF-FH-TAZ SA-ires-blast lentivirus vectors with blasticidin selection. C2C12 cells were passaged in growth medium (DMEM containing 10% FBS) and differentiated in C2C12 differentiation medium containing DMEM and 2% horse serum (Invitrogen). C2C12 cells in which TAZ was stably knocked down were prepared with pQCXI-GFP-2A-sh mouse TAZ retrovirus. To stably knock down LATS1 and LATS2 in MCF10A-TAZ cells, the cells were infected with pLenti-EmGFP-LATS1/2 KD lentivirus and GFP-positive cells were collected by fluorescence-activated cell sorting.

Quantitative RT-PCR. Quantitative RT-PCR analysis was performed with SYBR green (Roche) and the ABI7500 real-time PCR system (Applied Biosystems) (44). For the primers used, see Table S1 in the supplemental material.

RNAi. Human TAZ and mouse TAZ were knocked down in MCF10A and C2C12 cells as described previously (44). The double-stranded RNAs (dsRNAs) used were human TAZ s24789 (Ambion) and mouse TAZ siRNA D-041057 (Dharmacon). Knockdown was confirmed by quantitative RT-PCR or immunoblotting.

Myofusion index. C2C12 cells were fixed and immunostained with anti-MHC antibody. Nuclei were visualized with Hoechst 33342. The fusion index was calculated as a percentage of the nuclei detected within MHC-positive multinuclear cells.

Reporter assay. The TEAD reporter assay was performed with HEK293 cells as described previously (43). C2C12 cells were plated at 1×10^5/well in 12-well plates and cultured overnight. The cells were transfected with the pGL3 Myo-184 (MyoD), 8×GT-IIC-δ51LucII (for TEAD), 9×CAGA-MLP (for SMAD), and $p(PRS\text{-}1/\text{-}4)_3$ (for Pax3) luciferase reporter vectors alone or with TAZ. These reporter vectors were from Kenji Miyazawa (Yamanashi University), Hiroshi Sasaki (Ku-

mamoto University), and Hiroki Kurihara (The University of Tokyo) (37, 47, 48). Dimethyl sulfoxide (DMSO) or 10 μM IBS008738 was added 6 h after transfection. The cells were grown to confluence, transferred to differentiation medium with DMSO or 10 μM IBS008738, and cultured for 24 h before luciferase assays were performed.

ChIP analysis. Chromatin immunoprecipitation (ChIP) experiments were based on the protocol described by Nelson et al. (49). In brief, C2C12 myoblasts were cultured to confluence and then treated with DMSO or 10 μM IBS008738 in differentiation medium for 24 h. Cells were cross-linked in 1.42% (vol/vol) formaldehyde for 15 min, and the reaction was quenched for 5 min with 125 mM glycine. Cross-linked cells were lysed in buffer (50 mM Tris-HCl [pH 7.5], 150 mM NaCl, 5 mM EDTA, 0.5% [vol/vol] Nonidet P-40, 1% [vol/vol] Triton X-100), and chromatin was sheared by 25 consecutive rounds in a sonicator bath (Bioruptor; Diagenode) at maximum output and cycles of 30 s on and 60 s off. Shearing was analyzed by agarose gel electrophoresis. Chromatin from about 2×10^6 cells was incubated for 3 h at 4°C with 2 μg of antibodies. Immunoprecipitation was done with 20 μl of protein G-Sepharose beads. Protein G-Sepharose without antibody was used as the control (mock ChIP). The immunoprecipitated DNA fragments were isolated with Chelex-100 resin and diluted 1:2.5 for quantitative PCR analysis. Input-normalized relative abundance was determined. For the sequences of the primers used, see Table S1 in the supplemental material.

Subcellular fractionation. Subcellular fractionation was performed as described previously (43).

Myostatin inhibition assay. C2C12 cells were transfected with control or TAZ dsRNA. Forty-eight hours later, the cells were plated in growth medium at 2×10^5/well in 12-well plates. When grown to confluence, the cells were transferred to differentiation medium with DMSO, 100 ng/ml myostatin, 10 μM IBS008738, or a combination of myostatin and IBS008738 and cultured for 3 days. The differentiation medium containing the reagents was changed every day.

Cell proliferation and viability assessment. Cell proliferation and viability were assessed by MTT formazan dye conversion.

Sphere formation assay and 3D Matrigel culture. MCF10A and A431 cells were plated at 300/well in 96-well Ultra Low Attachment plates (Corning) and cultured for 10 days in serum-free DMEM–F-12 (Invitrogen) containing 10 ng/ml basic fibroblast growth factor, 20 ng/ml epidermal growth factor, 5 μg/ml insulin, and 0.4% (wt/vol) bovine serum albumin. A cell aggregate with a diameter of more than 150 μm was defined as a sphere. For three-dimensional (3D) Matrigel culture, 96-well plates were precoated with 30 μl of Matrigel per well. Cells were suspended at 2.1×10^6/liter in medium containing 2% Matrigel. Cell suspension volumes of 140 μl containing 300 cells were plated into each well and cultured for 10 days with DMSO or 10 μM IBS008738.

Animals. All experimental procedures were approved by the Institutional Animal Care and Use Committee. Six-week-old female BALB/cByJ mice (Clea Japan Inc.) were used. *N. mossambica* cardiotoxin was dissolved in phosphate-buffered saline (PBS) at a final concentration of 10 μM. A 100-μl volume of cardiotoxin solution was injected with either control DMSO or 3 nmol of IBS008738 (0.3 μl of DMSO or 0.3 μl of 10 mM IBS008738 was diluted in 100 μl of PBS) into the tibialis anterior (TA) muscle of mice ($n = 6$) under anesthesia. Mice were sacrificed on days 2, 5, 7, and 14. For dexamethasone-induced muscle atrophy, dexamethasone (25 mg/kg/day) or DMSO was injected intraperitoneally from day 1 to day 7. A 100-μl volume of 30 μM IBS008738 or DMSO in PBS was injected into the TA and gastrocnemius (GM) muscles on days 9, 11, and 13. Mice were sacrificed on day 14.

Skeletal muscle histology. TA and GM muscles were fixed in 4% formalin and embedded in paraffin. Muscle sections 5 μm thick were stained with hematoxylin and eosin. For the immunostaining of Pax7, MyoD, and laminin, 10-μm frozen sections were fixed with acetone at −20°C for 10 min, incubated with primary antibodies at 4°C overnight, and then visualized with secondary antibodies. To quantify the extent of muscle regeneration, four sections of each muscle at 100-μm intervals were analyzed and the total number of centrally nucleated myofibers per visual field was determined manually. To assess muscle atrophy, muscles were sectioned at a 10-μm thickness and immunostained with anti-laminin antibody. The cross-sectional areas of myofibers were analyzed by using the ImageJ software.

Phosphate affinity SDS-PAGE. Phosphate affinity SDS-PAGE was performed with Phos-tag acrylamide (Wako Chemicals) and polyvinylidene difluoride (PVDF) membranes.

***In vivo* SUnSET technique.** *In vivo* SUnSET was used according to the previously reported protocol (50). Briefly, mice were anesthetized and intraperitoneally injected with 0.04 μmol/g puromycin in 100 μl of PBS. Thirty minutes later, GM muscles were removed and frozen in liquid N_2. Frozen tissues were homogenized in buffer containing 40 mM Tris-HCl at pH 7.5, 0.5% (wt/vol) Triton X-100, 1 mM EDTA, 5 mM EGTA, 25 mM β-glycerophosphate, 25 mM NaF, 1 mM Na_3VO_4, 10 mg/liter leupeptin, and 1 mM phenylmethylsulfonyl fluoride. Sixty-microgram samples of total proteins were analyzed by SDS-PAGE, and immunoblotting with antipuromycin antibody was performed with PVDF membranes. The membranes were stained with Coomassie brilliant blue.

Statistical analysis. Statistical analyses were performed with Student's *t* test for the comparison of two samples and analysis of variance with Dunnett's test for multiple comparisons with GraphPad Prism 5.0 (GraphPad Software).

Other procedures. Immunoprecipitation and immunofluorescence assay were performed as described previously (51).

RESULTS

Cell-based assay to screen for the chemical compounds that activate TAZ. We used immortalized human mammary epithelial MCF10A cells to screen for TAZ activators. LATS1- and LATS2-dependent phosphorylation at serine 89 is the key event in the regulation of TAZ. Neither parent MCF10A cells nor MCF10A cells expressing TAZ (MCF10A-TAZ) survive under mammosphere-forming conditions, while MCF10A cells expressing S89A mutant TAZ (MCF10A-TAZ SA) do form spheres (Fig. 1A). However, with LATS1 and LATS2 knockdown, MCF10A-TAZ cells, but not parent MCF10A cells, form spheres (Fig. 1B). The additional knockdown of TAZ abolished the effect of LATS1 and LATS2 knockdown in MCF10A-TAZ cells (Fig. 1C and D). These findings indicate that sphere formation by MCF10A-TAZ cells reflects the activity of overexpressed TAZ.

The screening of 18,458 chemical compounds yielded 50 TAZ activator candidates. We cultured MCF10A-TAZ cells under sphere-forming conditions with 18,458 chemical compounds at 10 μM for 14 days. Fifty compounds enabled MCF10A-TAZ cells to form spheres (we defined a cell aggregate with a longest diameter of >150 μm as a sphere). We next performed the TEAD reporter assay with these 50 compounds. Forty-seven compounds enhanced TAZ-dependent TEAD reporter activity (data not shown).

TAZ activators enhanced myogenesis in C2C12 cells. TAZ plays important roles in the regulation of osteogenesis, adipogenesis, and myogenesis (34, 52). Here we focused on myogenesis and applied 50 compounds to mouse C2C12 myoblast cells. C2C12 cells were cultured under growth conditions. After grown to confluence, the cells were switched to differentiation conditions and cultured for 72 h in differentiation medium containing 10 μM each compound. We evaluated myogenesis by determining the myofusion index (the number of nuclei detected in multinuclear MHC-positive cells divided by the total number of nuclei). Cells treated with 43 compounds exhibited higher myogenesis than control cells (data not shown). In this study, we focused on one

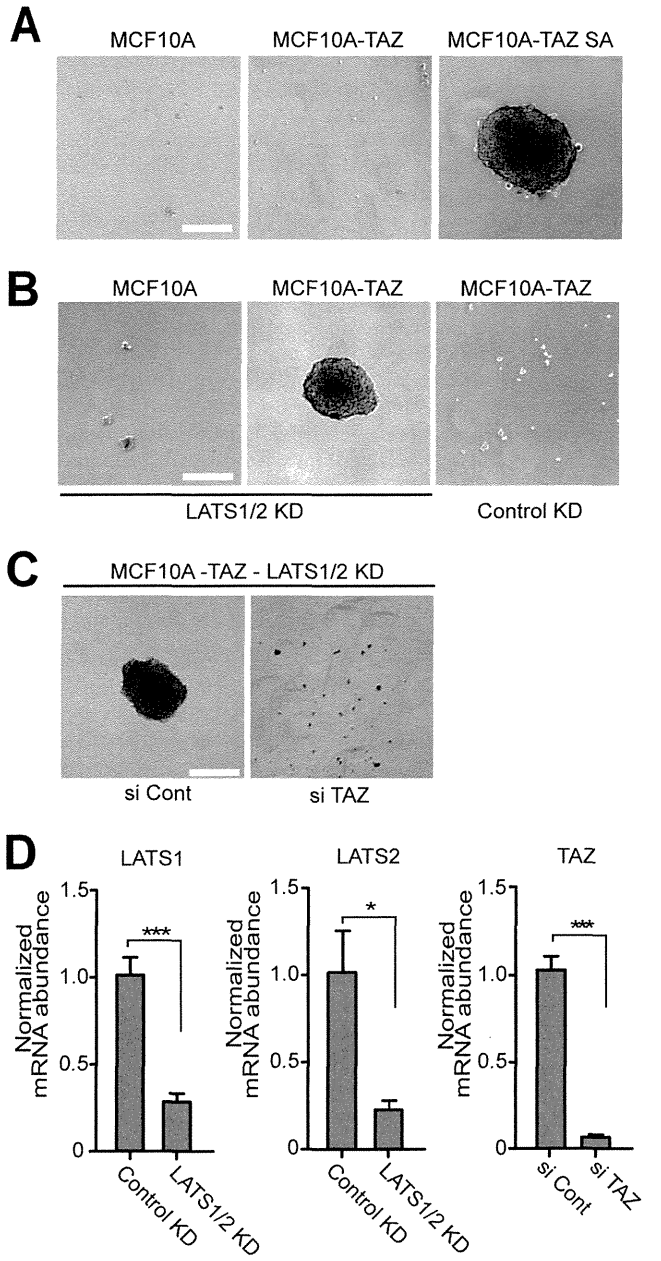

FIG 1 MCF10A cells form mammospheres depending on TAZ activity. (A) Parent MCF10A cells, TAZ-expressing MCF10A cells (MCF10A-TAZ), and TAZ SA-expressing MCF10A cells (MCF10A-TAZ SA) were cultured under mammosphere-forming conditions. Only MCF10A-TAZ SA formed spheres. (B) LATS1 and LATS2 were knocked down in parent MCF10A and MCF10A-TAZ cells. LATS1 and LATS2 knockdown (KD) provided MCF10A-TAZ cells with the capacity to form mammospheres. Parent MCF10A cells could not form mammospheres even with LATS1 and LATS2 knockdown. (C) Additional knockdown of TAZ in MCF10A-TAZ cells with LATS1 and LATS2 knockdown abolished the mammosphere formation induced by LATS1 and LATS2 knockdown. si Cont, control dsRNA; si TAZ, TAZ dsRNA. Bars, 200 μm. (D) Validation of LATS1, LATS2, and TAZ knockdowns in MCF10A cells. Data are means and standard errors of the means. *, $P < 0.05$; ***, $P < 0.001$.

compound named IBS008738, which showed the most significant effect (Fig. 2A). IBC008738 facilitated myogenesis and enhanced MHC expression (Fig. 2B). The effect was also detectable at 1 μM (Fig. 2C).

IBS008738 enhances protein expression of myogenic differentiation, and its effect depends on TAZ. When C2C12 cells were cultured with IBS008738 under growth conditions for 24 h and transferred to differentiation conditions, MyoD expression was slightly higher at 0 h (Fig. 2D). This finding suggests that IBS008738 has some ability, if not a significant one, to promote MyoD expression under growth conditions. MyoD expression more clearly increased at 24 and 48 h and declined at 72 h. Myogenin became detectable at 24 h in both control and IBS008738-treated cells, and IBS008738 increased its expression. An MHC signal started to be visible at 24 h in IBS008738-treated cells and was more apparent at 48 and 72 h than in control cells. IBS008738 also enhanced TAZ expression, with a peak at 24 h. It slightly facilitated the decrease in Pax7 but had no effect on Pax3. We knocked down endogenous TAZ with a dsRNA or shRNA retrovirus vector and confirmed that TAZ knockdown abolished the effect of IBS008738 (Fig. 2E and F).

IBS008738 enhances mRNAs of myogenic markers but not of myofusion markers. In a quantitative real-time PCR assay, the levels of transcription of the genes for myogenin and MyoD at 24 h under differentiation conditions were higher in IBS008738-treated cells but the differences were no more significant at 72 h (Fig. 3A). In contrast to TAZ protein expression, TAZ gene expression was not changed at 24 h and was reduced at 72 h. We tested the effect of IBS008738 on the expression of the genes that are regarded as TAZ targets in epithelial cells. The connective tissue growth factor (CTGF)- and cyclin D1-encoding genes were not increased in C2C12 cells by IBS008738 treatment (Fig. 3A). IBS008738 did not enhance but rather suppressed the genes for myofusion markers, including M-cadherin, calpain 1, and caveolin 3, which suggests that the enhanced myofusion observed in IBS008738-treated C2C12 cells reflects the facilitation of myogenesis at an early stage and is not directly driven by an enhanced fusion process (Fig. 3A).

IBS008738 enhances the MyoD-responsive myogenin promoter reporter in C2C12 cells. We tested whether and how IBS008738 affects the reporter activities regulated by various TAZ-interacting transcriptional factors in C2C12 cells. We exogenously expressed each reporter and TAZ in C2C12 cells and treated them with DMSO or IBS008738. TAZ overexpression enhanced the activities of all reporters, including the MyoD, TEAD, SMAD, and Pax3 reporters (Fig. 3B, first and the second columns). IBS008738 further enhanced only the MyoD reporter in C2C12 cells (Fig. 3B, second and third columns). In contrast to the result in HEK293 cells, IBS008738 did not enhance TEAD reporter activity in C2C12 cells. It did not enhance the effect of TAZ on the SMAD or Pax3 reporter either.

IBS008738 increases the association of MyoD with the myogenin promoter. MyoD, TEAD4, and Pax3 were immunoprecipitated from differentiated C2C12 cells treated with the control DMSO or IBS008738, and ChIP assays were performed. IBS008738 enhanced MyoD binding to the myogenin promoter but had no effect on the association of TEAD4 with the CTGF promoter (Fig. 3C). IBS008738 reduced the binding of Pax3 to the Myf5 promoter (Fig. 3C).

IBS008738 enhances the interaction of TAZ and MyoD. We tested the effect of IBS008738 on the interaction between TAZ and MyoD by immunoprecipitating endogenous TAZ from C2C12 cells. When MyoD was immunoprecipitated from C2C12 cells, IBS008738 slightly increased the amount of TAZ coimmunoprecipitated (Fig. 4A). However, as IBS008738 increased the expres-

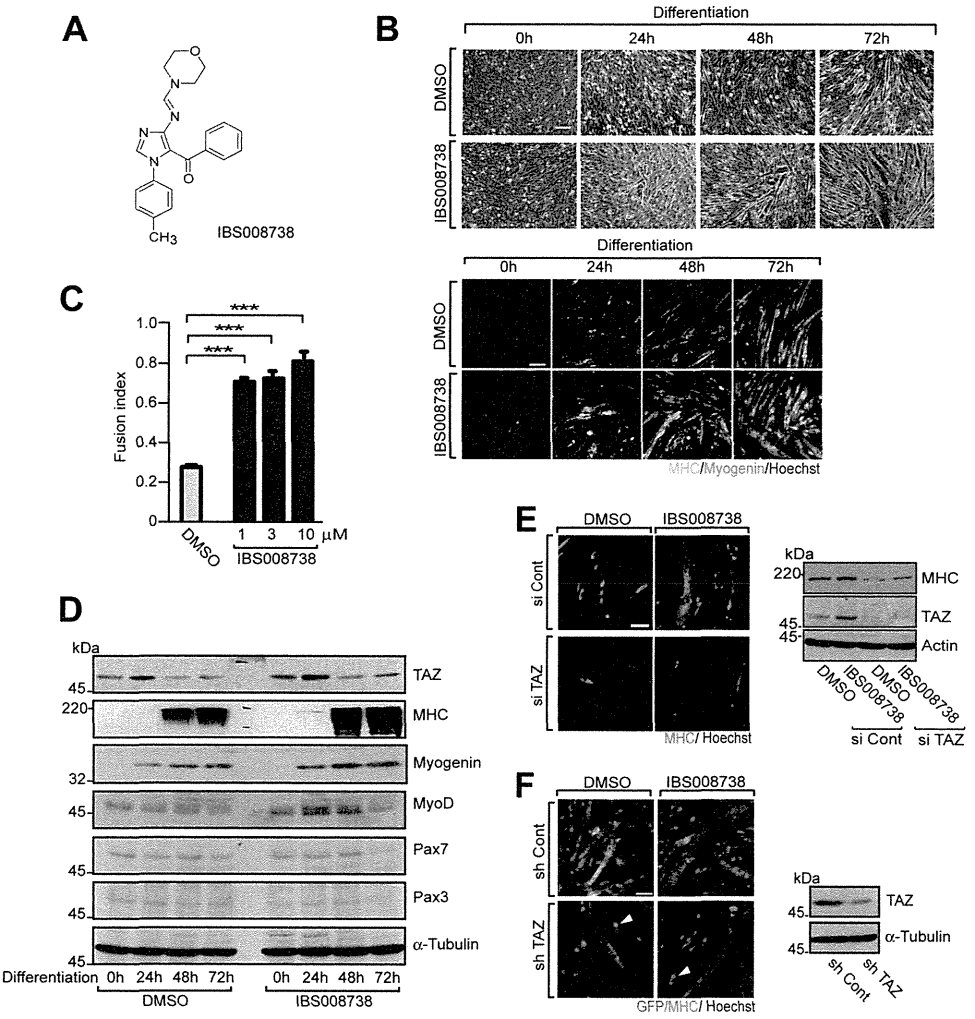

FIG 2 The TAZ activator candidate compound IBS008738 facilitates C2C12 myogenesis. (A) Chemical structure of IBS008738. (B) Phase-contrast images and immunofluorescence assays of C2C12 cells treated with DMSO or IBS008738. IBS008738 at 10 μM was added after the cells were switched to differentiation conditions. Cells were fixed at the time points indicated and immunostained with anti-MHC (green) and antimyogenin (red) antibodies (lower panels). Nuclei were visualized with Hoechst 33342. Bars, 100 μm. (C) C2C12 cells were treated with various doses of IBS008738. Myogenesis was evaluated by determining the myofusion index at 72 h. Data are means and standard errors of the means. ***, $P < 0.001$. (D) C2C12 cells were treated with DMSO or IBS008738 under growth conditions for 24 h, switched to differentiation conditions, and cultured for the indicated time periods with IBS008738 under differentiation conditions. The cells were harvested immediately after culture under growth conditions (0 h) or after 24, 48, or 72 h of culture under differentiation conditions. The lysates were immunoblotted with the antibodies indicated. α-Tubulin was used as the loading control. (E) C2C12 cells were transfected with control dsRNA (si Cont) or TAZ dsRNA (si TAZ). The cells were treated with DMSO or IBS008738 and fixed at 72 h under differentiation conditions. MHC was immunostained (red). The lysates were immunoblotted with anti-MHC and anti-TAZ antibodies. TAZ knockdown suppressed MHC expression in cells treated with DMSO (lane 3). TAZ knockdown abolished the effect of IBS008738 (lane 4). Immunoblotting with anti-TAZ antibody demonstrates that TAZ was efficiently knocked down. Bars, 100 μm. (F) Endogenous TAZ was suppressed by using shRNA in DMSO- and IBS008738-treated C2C12 cells. The retrovirus shRNA vectors harbor GFP as a tracer. MHC (red) expression is reduced in cells transfected with TAZ shRNA (green, arrowheads). The panel on the right shows the validation of shRNA.

sion of endogenous MyoD, the amount of MyoD immunoprecipitated itself increased. To circumvent this issue, we expressed FLAG-TAZ and HA-MyoD in HEK293 cells and performed immunoprecipitation with anti-FLAG M2 affinity gel. Under IBS008738 treatment, the interaction of HA-MyoD with FLAG-TAZ was enhanced (Fig. 4B, arrowhead). In the immunofluorescence of C2C12 cells, both endogenous MyoD and TAZ were diffusely distributed in the nucleus under growth conditions but formed dots under differentiation conditions (Fig. 4C, DMSO, top and middle). Interestingly, the expression of TAZ and MyoD was not the same in all of the cells. Some cells strongly expressed TAZ (red), whereas other cells expressed more MyoD (green) at 24 h after differentiation (Fig. 4C, middle). This finding is reminiscent of the previously reported heterogeneity of Myf5 expression and may suggest that MyoD and TAZ expression fluctuates like that of Myf5 in C2C12 cells (53). At 72 h in single-nucleus cells, TAZ expression decreased but MyoD was still expressed, while in multinuclear cells, both TAZ and MyoD were expressed and colocalized (yellow) in the nuclei (Fig. 4C, DMSO, bottom). IBS008738 did not have a significant effect under growth conditions. However, at 24 h under differentiation conditions, IBS008738 promoted the colocalization of TAZ and MyoD in single-nucleus cells and generated cells with two or three nuclei (Fig. 4C, IBS008738, middle, arrowheads). At 72 h, IBS008738 signifi-

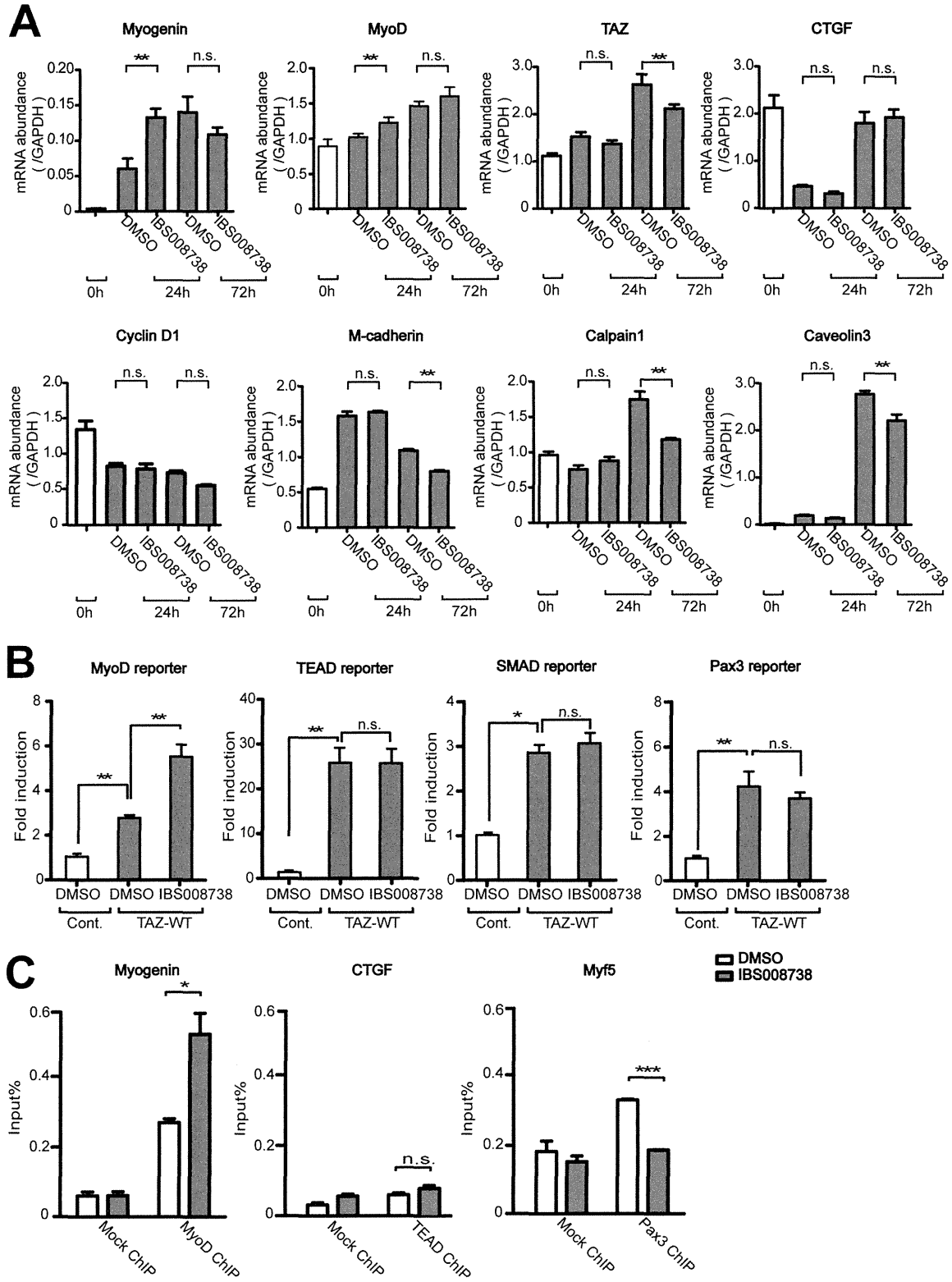

FIG 3 (A) IBS008738 enhances mRNAs of myogenic markers but not of myofusion markers. Quantitative RT-PCR was performed with mRNAs from C2C12 cells just before myogenesis induction (0 h) and from C2C12 cells treated with DMSO or IBS008738 for 24 or 72 h after myogenesis induction (24 h and 72 h). PCR was performed for myogenic markers (myogenin and MyoD), TAZ, putative targets of TAZ (CTGF and cyclin D1), and myofusion markers (M-cadherin, calpain 1, and caveolin 3). (B) IBS008738 enhances the MyoD-responsive myogenin promoter reporter in C2C12 cells. C2C12 cells were transfected with the pGL3 Myo-184-(MyoD), 8×GT-IIC-δ51LucII (for TEAD), 9×CAGA-MLP (for SMAD), and p(PRS-1/-4)3 (for Pax3) luciferase reporters alone (Cont) or with TAZ (TAZ-WT). The cells were grown to confluence and cultured for 24 h under differentiation conditions with DMSO or 10 μM IBS008738. (C) IBS008738 increases the association of MyoD with the myogenin promoter. C2C12 cells were cultured for 24 h under differentiation conditions. ChIP assay was performed with anti-MyoD (MyoD ChIP), anti-TEAD4 (TEAD ChIP), and anti-Pax3 (Pax3 ChIP) antibodies. PCR was performed to detect the promoters of myogenin, CTGF, and Myf5, respectively. Protein G-Sepharose was used as the control (Mock ChIP). In panels A to C, the data are means and standard errors of the means. *, $P < 0.05$; **, $P < 0.01$; ***, $P < 0.001$; n.s., not significant.

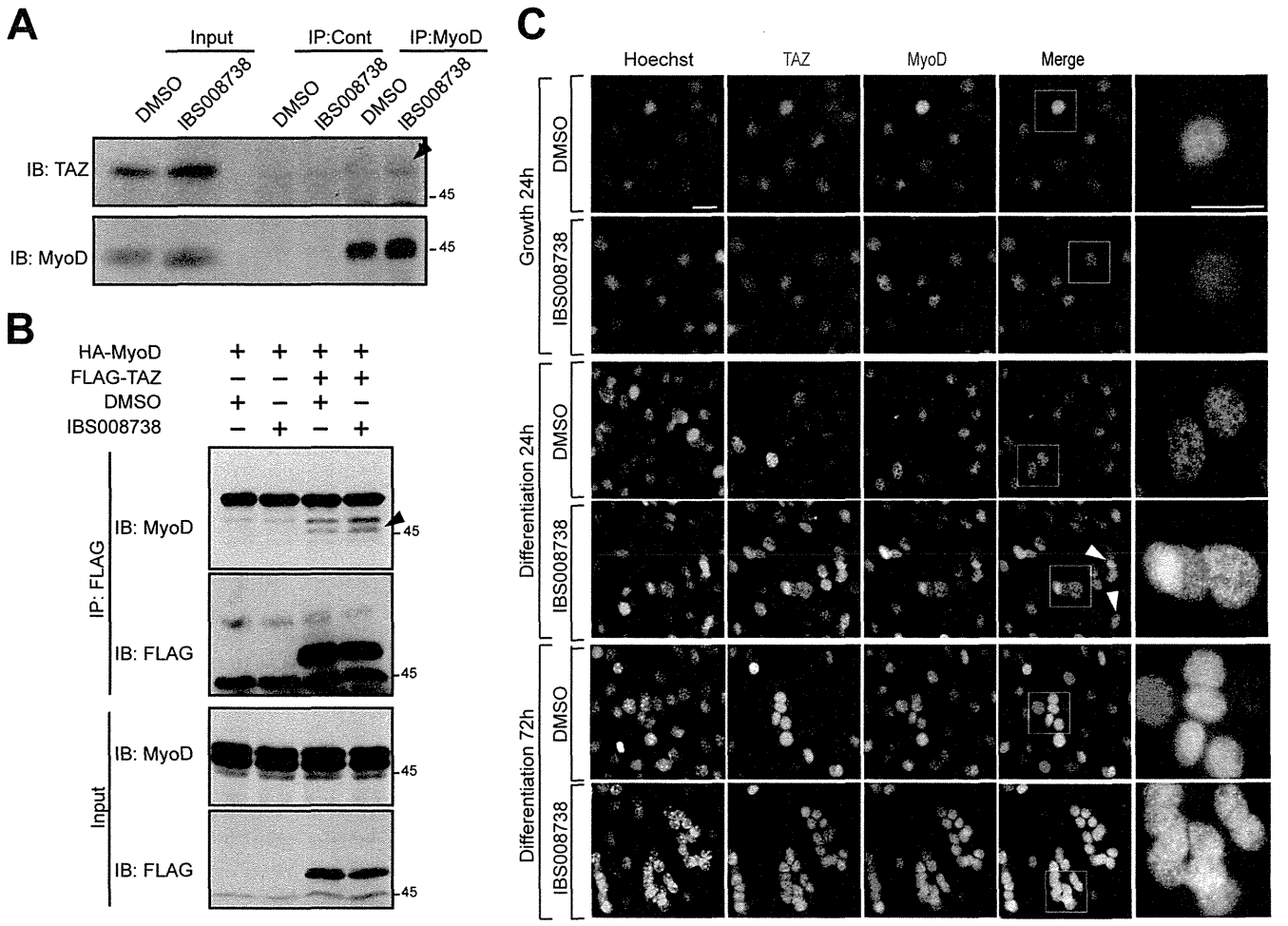

FIG 4 IBS008738 enhances the interaction between TAZ and MyoD. (A) MyoD was immunoprecipitated (IP) from DMSO- or IBS008738-treated C2C12 cells. The inputs and the precipitates were immunoblotted (IB) with anti-TAZ and anti-MyoD antibodies. TAZ immunoprecipitated from the IBS008738-treated cells increased (arrowhead). (B) HA-MyoD and FLAG-TAZ were expressed in HEK293 cells. Immunoprecipitation was performed with anti-FLAG M2 affinity gel. HA-MyoD was coimmunoprecipitated with FLAG-TAZ (third lane). IBS008738 increased the MyoD level in immunoprecipitates (arrowhead). (C) Endogenous MyoD and TAZ were immunostained in C2C12 cells at various stages. MyoD and TAZ were detected in the nuclei at all stages. Under growth conditions, both MyoD and TAZ were distributed diffusely in the nuclei. Under differentiation conditions, MyoD and TAZ formed dots in the nuclei. At 24 h after myogenesis induction, not all of the control cell nuclei expressed MyoD (green) and TAZ (red) equally. During treatment with IBS008738, the merged images are more yellowish, showing that MyoD and TAZ are better colocalized. Arrowheads indicate cells with two or three nuclei. Bar, 50 μm.

cantly increased the percentage of multinuclear cells (Fig. 4C, IBS008738, bottom).

IBS008738 increases the level of unphosphorylated TAZ in C2C12 cells. In epithelial cells, subcellular localization is important in TAZ activity regulation. However, consistent with the immunofluorescence results, in C2C12 cells, TAZ was detected mainly in the nuclear fraction and IBS008738 showed no significant effect on subcellular localization (Fig. 5A). To further characterize the effect of IBS008738 on TAZ, we analyzed TAZ by phosphate affinity SDS-PAGE. TAZ with serine 89 unphosphorylated, which was detected by anti-TAZ antibody (Fig. 5B, left) but not with antibody specific for TAZ with serine 89 phosphorylated (Fig. 5B, right), slightly increased (Fig. 5B, an arrow). However, phosphorylated TAZ also slightly increased, which means that IBS008738 increases the total amount of TAZ. Moreover, phosphorylated and unphosphorylated TAZ from IBS008738-treated cells exhibited mobility different from that of TAZ from control C2C12 cells (Fig. 5B, arrowhead). This finding suggests that in C2C12 cells, even TAZ with serine 89 unphosphorylated is localized in the nucleus and that IBS008738 induces some modification of TAZ, which is distinct from the phosphorylation at serine 89. We also tested the stability of TAZ. In control C2C12 cells, TAZ gradually decreased when protein synthesis was blocked by cycloheximide (Fig. 5C, DMSO). In IBS008738-treated C2C12 cells, TAZ expression was increased and degradation was delayed (Fig. 5C, IBS008738). IBS008738 is likely to stabilize TAZ.

Effect of IBS008738 on TAZ in MCF10A cells. As we used MCF10A cells in the original screening, we wanted to know whether IBS008738 has a similar effect on TAZ in MCF10A cells. The knockdown of TAZ in MCF10A-TAZ cells blocked sphere formation during treatment with IBS008738 (data now shown). Therefore, IBS008738-induced sphere formation indeed depends on TAZ. In the subcellular fractionation of MCF10A-TAZ cells that were cultured under sphere-forming conditions, IBS008738 increased the amount of nuclear TAZ (Fig. 5D, arrowhead). In MCF10A-TAZ cells, IBS008738 enhanced CTGF-encoding gene

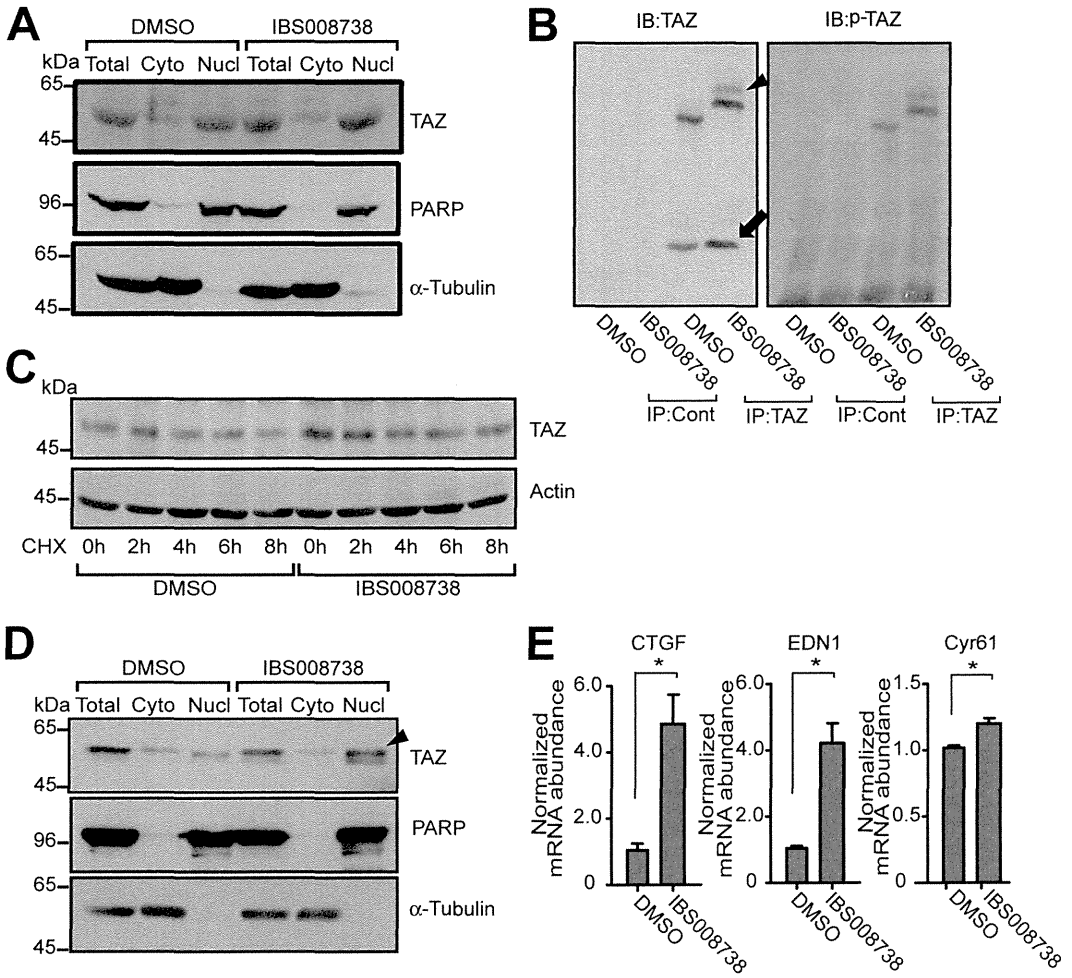

FIG 5 (A) Subcellular TAZ localization in C2C12 cells. Subcellular fractionation of C2C12 cells cultured for 24 h under differentiation conditions was performed. TAZ was recovered mainly in the nuclear fraction. IBS008738 did not significantly influence the distribution of TAZ. PARP and α-tubulin were used as nuclear and cytosolic markers, respectively. (B) TAZ was immunoprecipitated (IP) from lysates of DMSO- and IBS008738-treated C2C12 cells, analyzed by phosphate affinity SDS-PAGE, and immunoblotted with anti-TAZ antibody and anti-serine 89-phosphorylated TAZ-specific antibody, which recognizes the phosphorylation at serine 89. The lower band, which was detected by the anti-TAZ antibody but not by the anti-serine 89-phosphorylated TAZ-specific antibody, increased during treatment with IBS008738 (arrow). The upper bands, which were recognized by anti-serine 89-phosphorylated TAZ-specific antibody, exhibited a different mobility shift with IBS008738 treatment (arrowhead). (C) C2C12 cells were treated with DMSO or 10 μM IBS008738 for 24 h under differentiation conditions and then treated with 50 μg/ml cycloheximide (CHX). TAZ was immunoblotted at the time points indicated. TAZ expression gradually decreased in DMSO-treated C2C12 cells. TAZ expression increased in IBS008738-treated cells, and the decrease was delayed. (D) TAZ in the subcellular fractions of MCF10A-TAZ cells. TAZ was distributed equally in the cytoplasm and the nucleus. IBS008738 increased the nuclear TAZ level (arrowhead). (E) IBS008738 increased the levels of the mRNAs of the TAZ target genes for CTGF, EDN1, and Cyr61 in MCF10A cells. Data are means and standard errors of the means. *, $P < 0.05$.

transcription (Fig. 5E). It also enhanced EDN1 mRNA and to a lesser extent Cyr61 mRNA (Fig. 5E). These findings suggest that IBS008738 increases the nuclear TAZ level in both C2C12 and MCF10A cells but that the genes upregulated are determined in a cell context-dependent manner.

IBS008738 is most effective when applied for the first 24 h under differentiation conditions. To determine the stage at which IBS008738 influences myogenesis, we treated C2C12 cells with the compound at various time points. First, we treated C2C12 cells with various doses of IBS008738 under growth conditions, but IBS008738 had no effect on cell proliferation (Fig. 6A). Next we treated C2C12 cells for various times under differentiation conditions. Treatment during the first 24 h upregulated MHC (Fig. 6B). The expression of myogenin and MyoD was also enhanced (Fig. 6C, arrowheads). In contrast, treatment at 24 to 48 h or 48 to 72 h did not have a significant effect. These findings suggest that IBS008738 is most effective when it is applied during the initial phase of differentiation.

IBS008738 competes with myostatin. Myostatin is a member of the bone morphogenetic protein/transforming growth factor β superfamily and inhibits muscle growth and differentiation. It binds the activin type IIB receptor and triggers SMAD2- and -3-dependent signaling. As TAZ interacts with SMAD2 and -3, we wanted to know whether and how IBS008738 modulates myostatin signaling. Myostatin inhibited myogenesis in C2C12 cells, but IBS008738 restored myogenesis (Fig. 7A, si Cont). TAZ knockdown itself inhibited myogenesis and canceled the effect of IBS008738 (Fig. 7A, si TAZ). The myofusion index corroborated

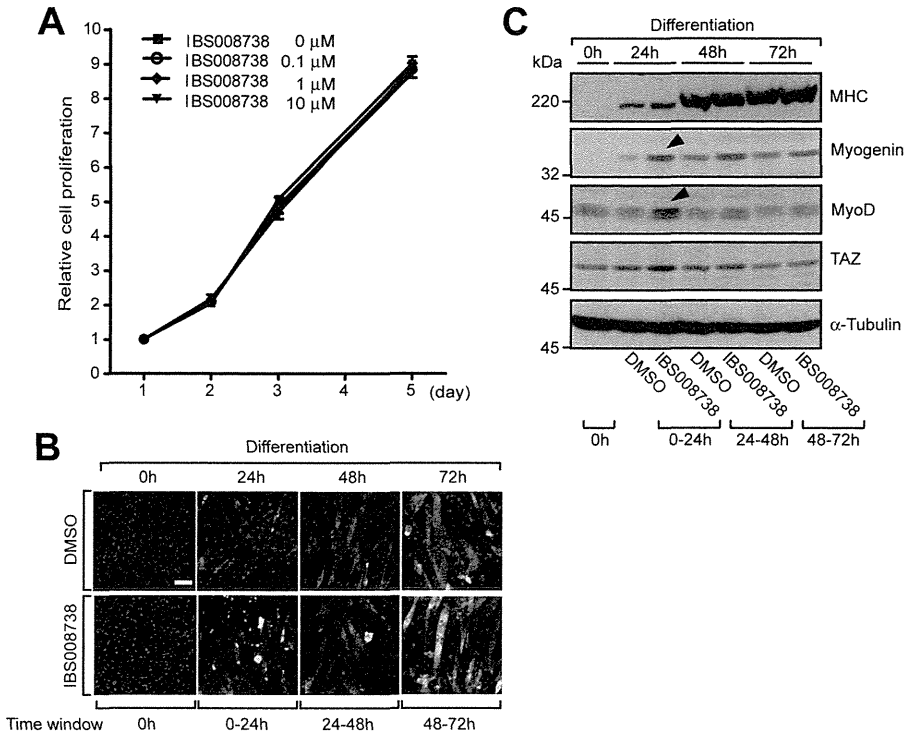

FIG 6 (A) C2C12 cells were cultured under growth conditions with various doses of IBS008738. Viable-cell numbers were evaluated by MTT assay. The value on day 1 after plating was set at 1. IBS008738 had no effect on cell proliferation. (B and C) C2C12 cells under differentiation conditions were treated with 10 μM IBS008738 during the time periods indicated (0 to 24, 24 to 48, and 48 to 72 h). Cells were harvested after treatment (at 24, 48, or 72 h). (B) Immunofluorescence images of MHC (white). Bar, 100 μm. (C) Immunoblotting of MHC, MyoD, myogenin, and TAZ. IBS008738 most significantly enhanced myogenin and MyoD when cells were treated during the first 24 h under differentiation conditions (arrowheads).

the immunofluorescence assay observation (Fig. 7B). In the immunoblotting assay, the MHC level decreased in myostatin-treated cells but IBS008738 restored it (Fig. 7C, second and third lanes). TAZ knockdown attenuated the restoration of MHC expression by IBS008738 (Fig. 7C, fifth and sixth lanes).

IBS008738 facilitates muscle repair in cardiotoxin-injected muscles. To assess the effect of IBS008738 on muscle regeneration, we injected cardiotoxin with control DMSO or IBS008738 into TA muscles. Hematoxylin-eosin staining showed that centrally nucleated fibers, a hallmark of regeneration, increased in IBS008738-injected muscles (Fig. 8A). To quantitatively evaluate muscle fiber size, we immunostained laminin, measured the sizes of myofibers demarcated by laminin, and confirmed the effect of IBS008738 (Fig. 8B). Pax7-positive cells, which were detected under the basal lamina, increased on day 5, decreased on day 7, and returned to the control level on day 14, whereas the number of MyoD-positive cells remained high on days 5 and 7 (Fig. 8C and D). All of these findings support the idea that IBS008738 facilitates muscle regeneration in response to injury.

IBS008738 prevents dexamethasone-induced muscle atrophy. We also induced muscle atrophy by dexamethasone administration in BALB/cByJ mice (n = 6 DMSO control, n = 6 dexamethasone treated) and injected IBS008738 three times into one hind limb muscle and control DMSO into the contralateral muscle. The mice were sacrificed on day 14. Dexamethasone treatment reduced muscle weights (Fig. 9A, first and third columns). IBS008738 did not increase muscle weights in control mice but prevented a dexamethasone-induced muscle decrease (Fig. 9A, second and fourth columns). Hematoxylin-eosin staining also showed a dexamethasone-induced reduction of muscle fiber size (Fig. 9B, upper panels). IBS008738 itself caused no significant change but prevented dexamethasone-induced muscle atrophy (Fig. 9B, lower panels). A quantitative evaluation of muscle fiber size confirmed the effect of IBS008738 (Fig. 9C). To measure protein synthesis, we injected puromycin 30 min before dexamethasone-treated mice were sacrificed and immunoblotted muscle lysates from the mice (n = 3 DMSO control, n = 3 IBS008738 treated) with antipuromycin antibody. IBS008738 significantly increased the incorporation of puromycin, suggesting that protein synthesis was enhanced in IBS008738-treated mice (Fig. 9D). Muscle-specific E3 ubiquitin ligases, MuRF-1, and atrogin-1 (MAFbx) are involved in glucocorticoid-induced muscle atrophy (54). Dexamethasone increased the MuRF-1 and atrogin-1 mRNA levels in GM muscles, but IBS008738 decreased them (Fig. 9E). These findings suggest that IBS008738 prevents dexamethasone-induced muscle atrophy through the inhibition of protein degradation and enhancement of protein synthesis.

IBS008738 does not significantly influence the malignant properties of cancer cells. We expect that IBS008738 is a promising lead compound for the development of a drug to prevent muscle atrophy and facilitate muscle regeneration after injury. However, TAZ is known as an oncogene and the hyperactivity of TAZ induces EMT of cancer cells. The effects of IBS008738 on the TEAD and SMAD reporters are not so significant in C2C12 cells, yet we need to consider the risk of IBS008738 application. We tested whether and how IBS008738 induces EMT in cancer cells. It

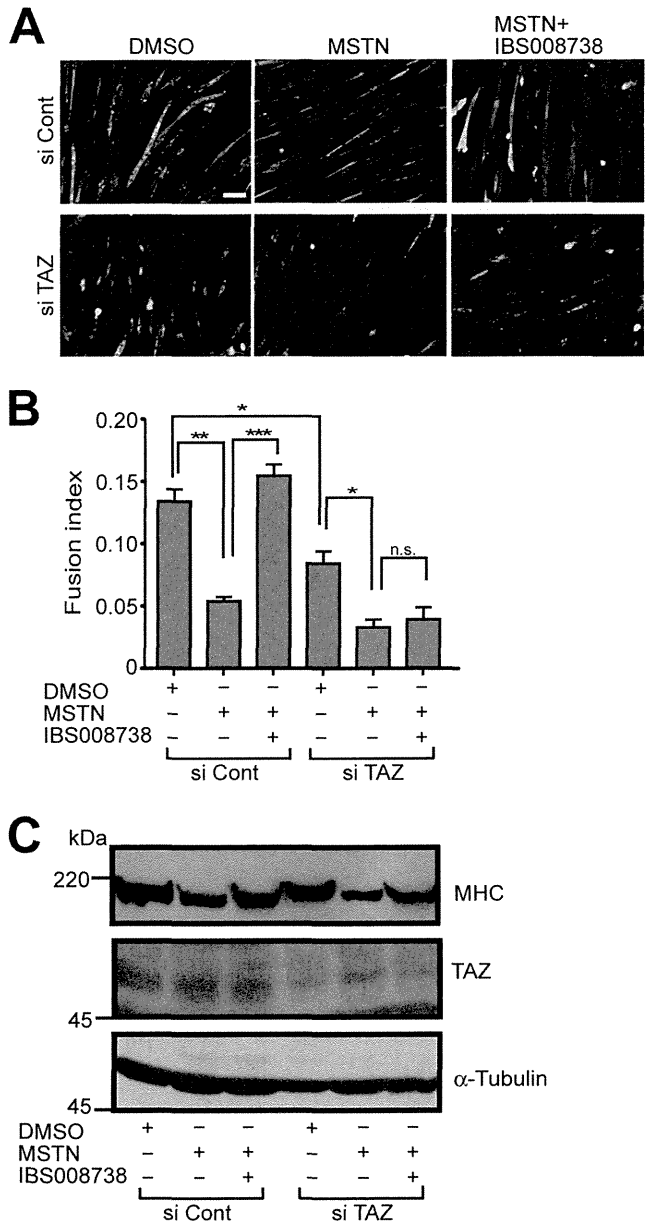

FIG 7 IBS008738 competes with myostatin. C2C12 cells were transfected with control dsRNA (si Cont) or TAZ dsRNA (si TAZ). Cells were grown to confluence and switched to differentiation conditions. Cells were cultured for 72 h with DMSO, 100 ng/ml myostatin (MSTN) alone, or 100 ng/ml myostatin with 10 μM IBS008738 as indicated. (A) Immunofluorescence images of MHC. Bar, 100 μm. (B) Myofusion index. Data are means and standard errors of the means. *, $P < 0.05$; **, $P < 0.01$; ***, $P < 0.001$; n.s., not significant. (C) Cell lysates were immunoblotted with the antibodies indicated.

did not enhance EMT marker protein expression in A431, A549, or HCT116 cells (Fig. 10A). IBS008738 did not enhance tumor sphere formation or the 3D Matrigel growth of A431 cells either (Fig. 10B).

DISCUSSION

In this study, we established a cell-based assay to search for TAZ activators. MCF10A-TAZ SA cells, which are unresponsive to negative regulation by the Hippo pathway, robustly form spheres under mammosphere-forming conditions, while parent MCF10A and MCF10A-TAZ cells lack the capacity to form spheres (Fig. 1). However, LATS1 and LATS2 knockdown makes MCF10A-TAZ cells, but not parent MCF10A cells, form spheres. The additional knockdown of TAZ in MCF10A-TAZ cells with LATS1 and LATS2 knockdown abolished sphere formation. These results indicate that MCF10A-TAZ cells acquire the capacity to form spheres when TAZ is activated. Therefore, we used this assay to identify compounds that activate TAZ. It is not clear which transcriptional factor is implicated in TAZ-dependent sphere formation by MCF10A cells. Among the TAZ-interacting transcriptional factors, TEAD proteins have been shown to be implicated in TAZ-mediated EMT (29). As EMT is related to stemness in cancer cells, genes transcribed by TEAD may be required for sphere formation. Most of the compounds obtained through this assay augment TAZ-dependent upregulation of TEAD-responsive reporter activity in HEK293 cells. The enhancement by the compounds is only 2-fold, but as cells are exposed to the compounds for a longer time in the sphere formation assay, the modest enhancement might be sufficient to induce sphere formation.

This assay gives compounds with disparate targets. The regulation of TAZ is multifaceted. The Hippo pathway, junction proteins, the actin cytoskeleton, and the Wnt pathway regulate TAZ. The compounds may upregulate TAZ through these regulatory mechanisms. Our preliminary experiments suggest that the compounds show different effects on the differentiation of mouse mesenchymal stem cells (data not shown). Some compounds strongly promote osteogenesis, while others do not. The inhibitory effects on adipogenesis are also unequal. These findings support the idea that each compound activates TAZ through a distinct mechanism. YAP1 is a paralog of TAZ. The molecular structures of YAP1 and TAZ are similar. YAP1 is regulated by the Hippo pathway, junction proteins, and the actin cytoskeleton in a manner similar to that of TAZ regulation (3, 12, 13). If the compounds work through the same regulatory mechanisms, the compounds should activate YAP1 too. Indeed, some of them enhance YAP1-dependent TEAD-responsive reporter activity, but not all of the compounds are active for YAP1. This observation also implies that the targets of 50 TAZ activator candidates are not the same. Thus, this new cell-based assay provided us with a collection of 50 TAZ activator candidate compounds that exhibit various cellular outputs and have distinct molecular targets.

As TAZ promotes osteogenesis and inhibits adipogenesis in mesenchymal stem cells, it is tempting to use TAZ activators therapeutically against osteoporosis and obesity. The osteogenic and antiadipogenic effects of kaempferol, a dietary flavonoid, depend on TAZ, supporting the notion that TAZ can be a therapeutic target in osteoporosis and obesity (55). Accordingly, the TAZ activator TM-25659 has been proposed to be beneficial in the control of osteoporosis and obesity (56). However, in the treatment of osteoporosis, the patients are females after menopause and relatively young. Once drug application starts, it is not easy to stop it. The oncogenic property of TAZ is an obstacle in the application of TAZ activators to osteoporosis. In the treatment of sarcopenia, the patients are extremely old. Once sufficient muscles are acquired for the rehabilitation program, the drug can be withdrawn. As the recovery of lower limb muscles is the most important, local application to those muscles by injection or percutaneously might be sufficient and systemic application could be avoided. Therefore, we expect that the treatment of sarcopenia with TAZ activators is

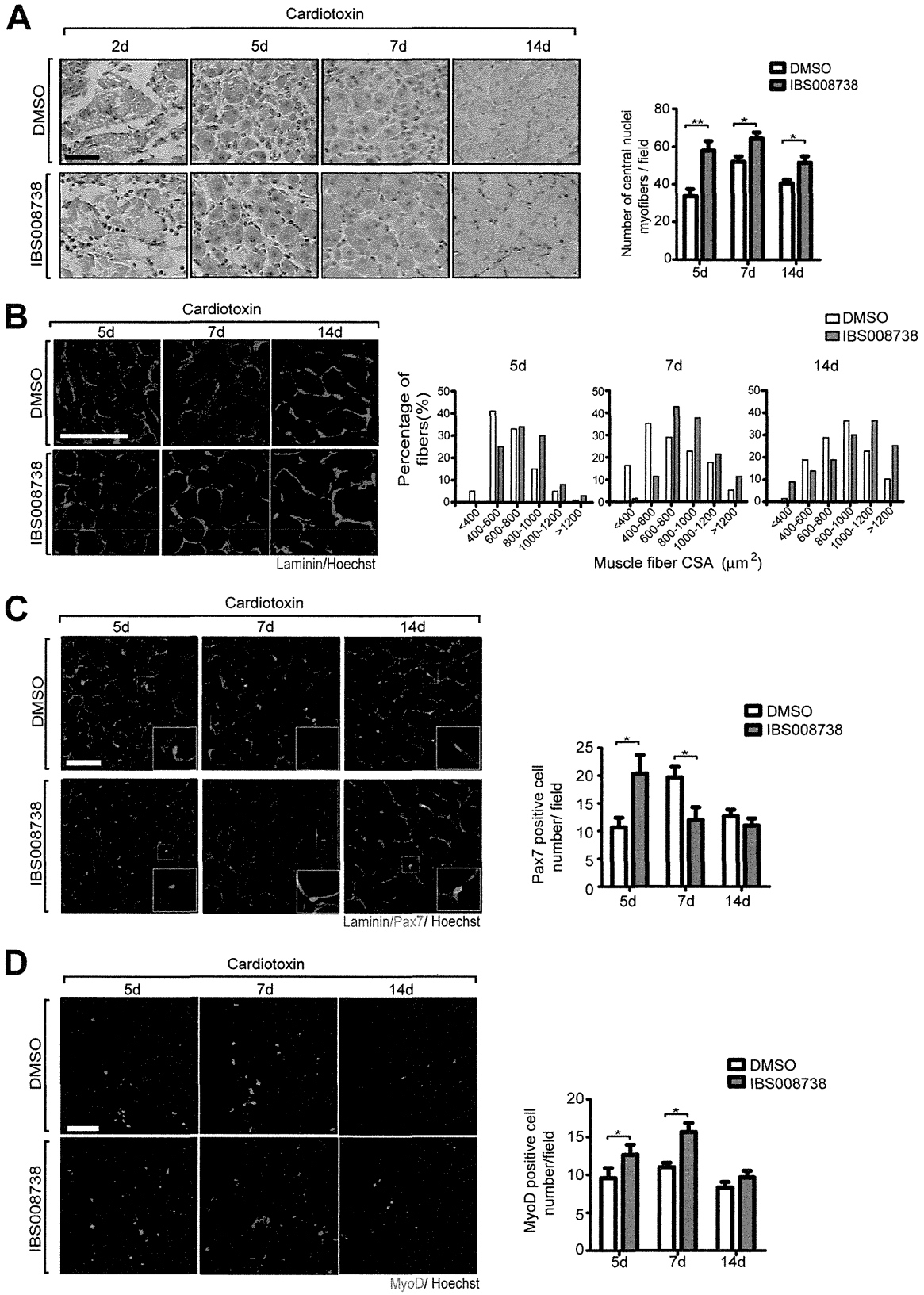

FIG 8 IBS008738 facilitates the repair of cardiotoxin-injected muscles. (A) Cardiotoxin was injected into TA muscles with control DMSO or IBS008738. The muscles were fixed at the time points indicated. The centrally nucleated fibers in nine independent fields of each muscle were counted at ×20 magnification. (B) Tissues were immunostained with antilaminin antibody. Cross-sectional areas (CSA) of myofibers were measured. Five hundred myofibers in each mouse sample were analyzed. Data from three mice are shown. (C and D) Tissues were immunostained with anti-Pax7 (red) and antilaminin (green) antibodies in panel C and with anti-MyoD antibody (red) in panel D at the time points indicated. In panel C, the marked fields are shown at higher magnification in the insets. The Pax7- and MyoD-positive cells in six independent fields of each muscle were counted at ×20 magnification. The data summarize the results obtained from three mice. In panels A, C, and D, the data are means and standard errors of the means. *, $P < 0.05$; **, $P < 0.01$. Bar, 50 μm.

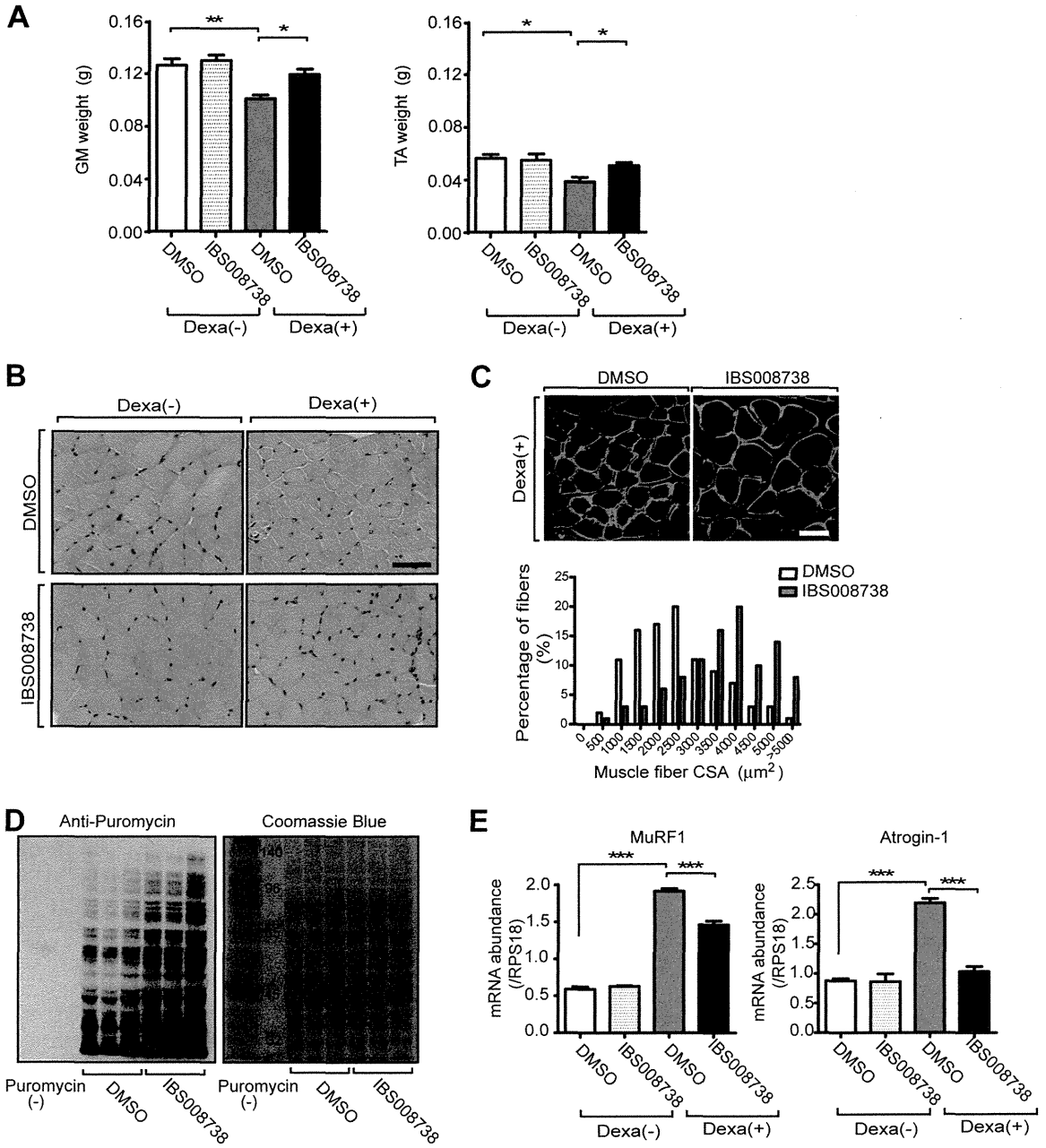

FIG 9 IBS008738 prevents dexamethasone-induced muscle atrophy. Dexamethasone (Dexa; 25 mg/kg/day) was intraperitoneally injected into 6-week-old female BALB/cByJ mice for 1 week. Control DMSO or IBS008738 was injected into their hind limbs every other day. On day 14, muscles were fixed. (A) Weights of GM and TA muscles. (B) Tissues were stained with hematoxylin and eosin. Dexamethasone induced muscle atrophy (upper panels). IBS008738 partially blocked atrophy (lower panels). Bar, 50 μm. (C) Cross-sectional areas (CSA) of myofibers were analyzed as described in the legend to Fig. 8B. (D) Puromycin was injected intraperitoneally 30 min before dexamethasone-treated mice were sacrificed. Puromycin-labeled proteins in GM muscles were detected with antipuromycin antibody (left panel). Samples of three DMSO-treated and three IBS008738-treated muscles were run side by side. A sample from a mouse with no injection of puromycin was run in the first lane. To confirm that the same amount of proteins was run in each lane, the membranes were stained with Coomassie brilliant blue (right panel). (E) Quantitative RT-PCR was performed with mRNAs from GM muscles. IBS008738 partially suppressed the dexamethasone-induced increase in the MuRF-1 and atrogin-1 mRNAs. In panels A and E, the data are means and standard errors of the means. *, $P < 0.05$; **, $P < 0.01$; ***, $P < 0.001$.

more realistic. Hence, we selected compounds that facilitate myogenesis in mouse C2C12 myoblast cells and expected that such compounds may also promote satellite cell proliferation and differentiation. In this study, we focused on one compound, IBS008738.

The effects of IBS008738 on sphere formation by MCF10A-TAZ cells and myogenesis of C2C12 cells are both abolished by TAZ knockdown. This indicates that the effect of IBS008738 depends on TAZ. In MCF10A-TAZ cells, IBS008738 increases the nuclear TAZ level (Fig. 5). In C2C12 cells, IBS008738 increases the